The dual trxG/PcG protein ULTRAPETALA1 modulates H3K27me3 and directly enhances POLYCOMB REPRESSIVE COMPLEX 2 activity for fine-tuned reproductive transitions

Subtitle: ULT1 differentially regulates H3K27me3 levels in a gene-specific manner, and functions as a cofactor of PRC2 to control key flowering genes

Vangeli Geshkovski[1,#], Julia Engelhorn[1,2,#,*], Jean-Baptiste Izquierdo[1,3,#], Hamida Laroussi[3,‡], Caroline Thouly[1,‡], Laura Turchi[1,‡], Marie Le Masson[1], Emmanuel Thévenon[1], Ambre Petitalot[4], Lauriane Simon[5], Sophie Desset[5], Philipp Michl-Holzinger[6], Hugues Parrinello[7], Klaus D. Grasser[6], Aline Probst[5], Raphaël Margueron[4], Gilles Vachon[1], Jan Kadlec[3,*] and Cristel C. Carles[1,*]

[1] Grenoble Alpes University, CNRS, INRA, CEA, Plant and Cell Physiology Lab (LPCV), Bioscience and Biotechnology Institute of Grenoble, CEA, 17 rue des Martyrs, bât. C2, 38054 GRENOBLE Cedex 9, France
[2]current address: DIADE, Université de Montpellier, IRD, CIRAD, Montpellier, France
[3]Grenoble Alpes University, CNRS, CEA, IBS, F-38000 Grenoble, France
[4] Institut Curie, Paris Sciences et Lettres Research University INSERM U934/CNRS UMR3215, Paris, France
[5] Institute of Genetics Reproduction and Development (iGReD), Université Clermont Auvergne, CNRS, Inserm, Clermont-Ferrand, F-63000, France.
[6] Cell Biology and Plant Biochemistry, University of Regensburg, D-93053 Regensburg, Germany.
[7] Cell MGX-Montpellier GenomiX, Univ. Montpellier, CNRS, INSERM, Montpellier, France.
[#] These authors contributed equally: Julia Engelhorn, Vangeli Geshkovski, Jean-Baptiste Izquierdo.
[‡] These authors contributed equally: Hamida Laroussi, Caroline Thouly, Laura Turchi.

[*]Correspondence: Christel.carles@univ-grenoble-alpes.fr, @Cristel_Carles
Jan.kadlec@ibs.fr
julia.engelhorn@umontpellier.fr

37 ***Key message:*** ULTRAPETALA1 counteracts or promotes PRC2 activity at hundreds of developmental
38 genes in *Arabidopsis thaliana*, and activates the deposition of the repressive H3K27me3 chromatin
39 mark via direct interaction with PRC2.
40 *This is the first instance of a bivalent trxG / PcG factor which functions as a cofactor of PRC2 HMTs.*

Abstract

The antagonistic POLYCOMB (PcG) REPRESSIVE COMPLEX 2 (PRC2) and trithorax (trxG) chromatin machineries play a major role in orchestrating gene expression during the development of multicellular eukaryotes. These complexes are well known for depositing and maintaining the repressive H3K27me3 and activating H3K4me3 marks, respectively. However, the mechanisms that govern the switch between these functions remains elusive, especially in plants, whose lifelong, flexible development relies heavily on this process. Here we demonstrate that the plant specific ULTRAPETALA1 (ULT1) protein, previously reported as a trxG factor that antagonizes the PRC2 enzymatic subunit CURLY LEAF (CLF), also exhibits a repressive function, increasing H3K27me3 levels at over a thousand genes. We discovered a physical interaction between ULT1 and PRC2 components, particularly the SWINGER (SWN) enzymatic subunit. We further show that ULT1 significantly enhances $PRC2^{SWN}$ enzymatic activity *in vitro*, corroborating our epigenomic and developmental genetic data that reveal different ULT1 activity depending on the catalytic subunit of the PRC2 complex. This study provides new insights into the relative activities of CLF and SWN and introduces a novel mechanistic framework for a chromatin switch mediated by a bivalent trxG/PcG factor.

Chromatin structure is intimately connected with gene expression and cell identity (Perino and Veenstra, 2016). Establishment of cell fates during development is accompanied by large-scale chromatin remodelling, which contributes to both lineage specification and maintenance. These epigenetic processes establish a chromatin framework that regulates the various developmental phases of multicellular eukaryotes.

Two antagonistic post-translational modifications carried by lysine residues of histone H3, H3K27me3 and H3K4me3, are key regulatory chromatin marks for genes of all higher eukaryotes (Kingston & Tamkun, 2014a; Mozgova & Hennig, 2015; Aranda *et al.*, 2015); Schuettengruber *et al.*, 2007). The Polycomb group (PcG) REPRESSIVE COMPLEX 2 (PRC2) and trithorax group (trxG) are responsible for the deposition of repressive and active trimethyl marks on H3K27 and H3K4, respectively. H3K27me3, in particular, is found at thousands of developmental genes, many of which are involved in cell fate determination, including differentiation and maintenance of cell identity.

In animals, loss of PRC2 function leads to aberrant gene expression often affecting the expression of *HOX* genes and impairing stem cells differentiation, as initially reported in Drosophila (Schuettengruber *et al.*, 2017). In plants, PRC2-mediated repression of MADS genes is essential for body and organ patterning, as well as developmental phase changes, throughout the lifespan. This is illustrated by the loss-of-function Arabidopsis mutants which display homeotic phenotypes and shifts in growth transitions(Engelhorn *et al.*, 2014). Until now the antagonism between PcG/PRC2 and trxG functions has been demonstrated unidirectionally through the suppression of PRC2 mutant phenotypes by mutations in trxG genes (Berr *et al.*, 2011; Kingston & Tamkun, 2014b).

Two PRC2 complexes are known in animals, containing the Enhancer of Zeste (E(z)) homolog 2 (EZH2) or the EZH1 enzyme, respectively, which catalyse di- or trimethylation of H3K27 (Margueron & Reinberg, 2011). Interestingly, EZH1 exhibits a lower enzymatic capacity than EZH2 (Margueron *et al.*, 2008) (Lee *et al.*, 2018). In Arabidopsis, there are three E(z) homologous PRC2 enzymatic subunits: one predominantly gametophytic, MEDEA (MEA), and two sporophytic, CURLY LEAF (CLF) and SWINGER (SWN), which catalyse all three levels of H3K27 methylation (Jacob *et al.*, 2014; Borg *et al.*, 2020). *In vitro* methylation assays have shown that MEA and CLF are active, however no data is available for SWN (Schmitges *et al.*, 2011; Jacob *et al.*, 2014; Borg *et al.*, 2020).

The apparent functions of the PRC2 sporophytic enzymes CLF and SWN, as revealed by loss-of-function mutants, are not equivalent: *clf* mutants show upward leaf curling, early flowering and flowers with homeotic defects. These phenotypes are largely caused by ectopic expression of the MADS floral genes *AGAMOUS (AG)* and *APETALA3* (*AP3)* (Goodrich *et al.*, 1997). Interestingly, although the *FLOWERING LOCUS C* (*FLC*) MADS gene, central repressor of flowering, is highly upregulated in *clf* mutants, these plants flower early, showcasing the complexity of the pleiotropic phenotypes of *prc2* mutants. For *swn*

91 mutants, plants are not clearly distinguishable from wild-type plants except for a slight flowering time
92 defect (Shu *et al.*, 2019). This was also observed at the molecular level, as very few genes show a
93 change in H3K27me3 or transcript levels in *swn* compared to wild-type plants (Shu *et al.*, 2019). *clf swn*
94 double mutants, however, develop callus-like masses of disorganized tissue after normal embryonic
95 development. These structures contain a multitude of tissue types resulting from uncontrolled cell
96 differentiation and due to ectopic de-repression of thousands of developmental genes(Chanvivattana
97 *et al.*, 2004).
98 The PRC2 complex of Drosophila comprises three other sub-units: Extra Sex Comb (ESC) or its homolog
99 ESCL; Suppressor of Zeste 12 (SU(Z)12) and p55 (Czermin *et al.*, 2002). While there is only one ESC
100 homolog in Arabidopsis, FERTILIZATION INDEPENDENT ENDOSPERM (FIE), there are three SU(Z)12
101 homologs: EMBRYONIC FLOWER 2 (EMF2), VERNALIZATION INSENSITIVE 2 (VRN2) and FERTILIZATION-
102 INDEPENDENT SEED 2 (FIS2); and five p55 homologues: MULTICOPY SUPPRESSOR OF IRA 1-5 (MSI1-5,
103 with only MSI1 demonstrated to be part of the PRC2 complex).
104
105 The regulation of PRC2 enzymatic activity in mammals has attracted considerable attention. It is
106 now well established that a set of cofactors interact with SU(Z)12 and are essential for the proper
107 targeting and activity of PRC2 (Højfeldt *et al.*, 2019). While most of these cofactors have paralogs in
108 Drosophila, the situation appears quite different in plants, where many PRC2 direct interactors are
109 unique to the green lineage (Godwin & Farrona, 2022). Moreover, the impact and mechanism of these
110 plant accessory proteins on the activities of PRC2 remain largely unknown.
111 We previously identified a PRC2 antagonist, called ULTRAPETALA1 (ULT1), that promotes
112 developmental switches such as floral transition and flower morphogenesis in *Arabidopsis thaliana*.
113 We found that ULT1 regulates stem cell maintenance and differentiation in the shoot apex, via
114 transcriptional regulation of developmental loci (Carles *et al.*, 2004, 2005). When ectopically expressed
115 in plants, it induces homeotic phenotypes through the ectopic expression of meristem and flower
116 MADS genes and reduction in H3K27me3 levels at these loci. Moreover, when combined with a
117 mutation in the PRC2 catalytic subunit CLF, *ult1* loss-of-function hides PRC2 mutant phenotypes (Carles
118 & Fletcher, 2009). This trxG-type of function of ULT1 was explained by the direct regulation of *AG* and
119 *AP3* (Carles & Fletcher, 2009).
120 On the other hand, ULT1 was also reported to have a Polycomb-type function. Indeed, ULT1 together
121 with the trxG ATX1 and PcG EMF1 members, prevent seed gene expression after germination (Xu *et*
122 *al.*, 2018). This contribution to seed gene repression in seedlings correlates with a decrease in
123 H3K27me3 levels, only observed in the specific genetic context of the *ult1 atx1 emf1* triple mutant.

124 Thus, while ULT1 derepresses flower genes, reducing their H3K27me3 levels, it contributes to
125 repression of seed genes, which associates with elevated H3K27me3 levels. These two sets of
126 seemingly contrasting findings position ULT1 as a potential dual regulator of chromatin dynamics.
127
128 To further investigate ULT1 opposing regulatory activities on PRC2, we employed a genome-wide
129 approach assessing the effect of ULT1 on the abundance of the H3K27me3 mark, using loss- and gain-
130 of-function lines. We found that, on one hand, ULT1 reduces H3K27me3 amounts at over a fourth of
131 CLF targets, and that these targets are enriched in transcriptional and developmental functions.
132 Interestingly, the targets for de-repression poorly overlap with targets of the H3K27me3 Histone
133 demethylases (HDMT) REF6, ELF6 and JMJ13. On the other hand, ULT1 promotes an increase in
134 H3K27me3 amounts at a third of genes known to be repressed by the other sporophytic H3K27 histone
135 methyltransferase (HMT), SWN. We found that ULT1 physically interacts with both CLF and SWN, with
136 a better affinity for SWN, and does not interfere with the PRC2 complex assembly. Moreover, we also
137 show that ULT1 significantly increases the *in vitro* HMT activity of the SWN-containing PRC2 complex.
138 Finally, phenotypic and molecular analyses of flowering time and flower organ number lead to a
139 consistent interaction with SWN, along with the co-regulation of key developmental target genes.

140 **Results**

141

142 **ULT1 has a dual genome-wide effect on H3K27me3 abundance**

143 To assess the effect of ULT1 on PRC2-induced H3K27me3 deposition, we quantified global and
144 genome-wide levels of H3K27me3 in the *ult1-2* and *ult1-3* loss-of-function lines(Carles *et al.*, 2005),
145 thereafter referred to as *ULT1* lof, as well as in a *35S::ULT1* gain-of-function line(Carles & Fletcher,
146 2009), thereafter referred to as *ULT1* gof. These experiments revealed that ULT1 has a dual effect on
147 H3K27me3 abundance, inducing both its decrease and increase at two distinct sets of genes.

148 *ULT1 negatively regulates H3K27me3 enrichment at 916 loci*

149 Chromatin immuno-precipitation assays followed by sequencing (ChIP-seq) revealed that 2925
150 genes show a consistent decrease of sequencing-depth-normalized H3K27me3 abundance in *ULT1* gof,
151 while 1532 and 1378 show an increase in *ult1-2* and *ult1-3* lof, respectively (Fig. 1A). 916 targets are
152 shared between these three sets of genes (Table S1), which we named ULT1_derep, as they are target
153 genes for de-repression by ULT1. The ULT1_derep population shows an enrichment in the Gene
154 Ontology (GO) development-related processes and transcription factors (Fig. 1B and Suppl. Fig.S1),
155 including meristem, flowering and flower morphogenesis regulators. Among these are the flower
156 MADS transcription factor-encoding genes, in particular *AGAMOUS* (*AG*), *APETALA3* (*AP3*) and
157 *SEPALLATA1-4* (*SEP1-4*), previously reported to be targets for activation by ULT1 (Carles & Fletcher,
158 2009). In addition to these already known targets, we found *AP1*, *CAULIFLOWER* (*CAL*), *PISTILLATA* (*PI*)
159 and the flowering regulators *AGAMOUS-LIKE 24* (*AGL24*) and *FLOWERING LOCUS T* (*FT*) (Fig. 1C; Suppl.
160 Fig. S2; Table S1). This dataset thus supports a model where ULT1 functions as a PRC2 antagonist.

161 *ULT1 positively regulates H3K27me3 enrichment at 1362 loci*

162 Remarkably, the ChIP-seq data also revealed an opposite effect of ULT1 on H3K27me3 abundance,
163 demonstrating that ULT1 functions also as a potent PRC2 agonist. Indeed, 4800 genes showing an
164 increase in *ULT1* gof, and 2670 and 2617 showing a decrease in *ult1-2* and *ult1-3* lof, respectively (Fig.
165 1A). The 1362 genes common to these three sets were named ULT1_rep (target genes for repression
166 by ULT1) (Table S1). GO analyses do not reveal enrichment in development-related processes and
167 transcription factors terms, even though the ULT1_rep genes comprise some flowering time and
168 meristem regulators. These include several developmental genes coding for transcription factors,
169 including the MADS gene *FLOWERING LOCUS C* (*FLC*), master regulator of the reproductive transition
170 and its two paralogues *MADS AFFECTING FLOWERING 4* (*MAF4*) and *MAF5*, *AGAMOUS-LIKE LOCUS 51*
171 (*AGL51*), the meristem regulators *AINTEGUMENTA-LIKE 7* (*AIL7*), *CUP-SHAPED COTYLEDON 1* (*CUC1*),
172 *ARABIDOPSIS PIN-FORMED 7* (*PIN7*) and *PERIANTHIA* (*PAN*) (Fig. 1C; Suppl. Fig. S2; Table S1). In
173 contrast to previously reported biologically relevant ULT1_derep targets (Carles & Fletcher, 2009; Pu

174 *et al.*, 2013), there is little evidence for ULT1 function as a repressor, except in the context of seed
175 germination(Xu *et al.*, 2018). We therefore confirmed the effect of ULT1 through ChIP-qPCR, on some
176 of the ULT1_rep genes (Suppl Fig. S3). Together, these results reveal that, in addition to reducing
177 H3K27me3 levels at many genes, ULT1 can also enhance the accumulation of this mark across a broad
178 set of genes.

179 *ULT1 impacts H3K27me3 throughout target loci and leads to overall H3K27me3 increase in the nucleus*

180 For both ULT1_derep and ULT1_rep genes, mark abundance changes can be observed throughout
181 the target loci (Fig. 1C-E; Suppl. Fig. S2). Hence, ULT1 impacts the entire H3K27me3-marked region of
182 genes it regulates.
183 Moreover, meta-gene analyses reveal an overall promoting function of H3K27me3 abundance by ULT1
184 (summed-up effect on all targets) (Fig. 1D, E). This global increase in H3K27me3 upon overexpression
185 of ULT1 can also be revealed by western-blots and by immunofluorescence staining (Fig. 1F, G; Suppl.
186 Fig. S4). Finally, a small decrease in the relative heterochromatin fraction in ULT1 gof reveals a
187 moderate effect on global nuclear organization (Suppl. Fig. S5). This implies that changes in H3K27me3
188 levels could influence organization of repetitive elements in chromocenters, chromocenter formation,
189 or global chromatin organization.

190 *ULT1 impacts fewer targets for H3K4me3 abundance and gene expression, yet changes occur for*
191 *common flowering and flower morphogenesis genes*

192 Next, we wanted to assess whether the changes we observed in H3K27me3 were correlated with
193 changes in the abundance of the antagonistic mark H3K4me3. We thus analysed H3K4me3 genome-
194 wide in the same ULT1 lof and ULT1 gof lines, using the same chromatin samples as those immuno-
195 precipitated for the H3K27me3 ChIP-seq experiments. We also assessed the correlation with gene
196 expression changes through RNA-seq experiments (Suppl Tables S2 and S3) on the same tissues.
197 We found that, compared to its effect on H3K27me3 levels, ULT1 has a less striking effect on the
198 abundance of the H3K4me3 mark and on gene expression (Suppl Fig. S1B,D; Suppl Fig. S6 and S7).
199 Indeed, only 45 genes show increase in the H3K4me3 mark in *ULT1* gof, and 6 genes show decrease in
200 the H3K4me3 mark in both *ULT1* lof lines. On the other hand, 117 genes show decrease in the
201 H3K4me3 mark in *ULT1* gof line, and 24 genes show increase in the H3K4me3 mark in both *ULT1* lof
202 lines (Suppl Fig. S6A). GO analyses reveal that the population of genes which lose the H3K4me3 mark
203 in ULT1 gof is enriched in development and cell fate specification related terms (Suppl Fig. S8).
204 Transcriptional analyses showed that 14 genes were down-regulated and 48 were up-regulated in both
205 ULT1 lof lines, while the *35S::ULT1* gof line had 136 up-regulated and 81 down-regulated genes (Suppl.
206 Fig. S7A,B).

207 Likely as a consequence of their smaller sizes, the populations of H3K4me3 differentially
208 methylated genes (DMG) or of differentially expressed genes (DEG), have a limited overlap with the
209 populations of H3K27me3 DMG (Suppl. Fig. S6 and S7). Yet, some specific genes that are biologically
210 relevant regarding ULT1 developmental functions, were shared between the datasets. Among the
211 ULT1_derep genes (identified previously based on H3K27me3 changes), 6 also showed elevated
212 H3K4me3 in *ULT1* gof, including *SEP3,* and 10 showed elevated expression in *ULT1* gof, including *SEP3*,
213 *FT* and *PI* (Table S3). On the other hand, *FLC,* which is part of ULT1_rep targets, is one of the very few
214 genes that also shows H3K4me3 increase in *ult1-2* lof and decrease in *35S::ULT1* gof, and significantly
215 and coherently changes in expression in our transcriptomic dataset, for all ULT1 lof and gof lines (Suppl.
216 Fig. S2B,D and Suppl. Tables S2 and S3).
217 Together, these findings show that ULT1 modulates H3K27me3 levels, either enhancing or
218 reducing them across broad gene sets, thereby acting as both an antagonist and agonist of PRC2.
219
220 **ULT1 de-represses mainly CLF targets, independently of JmJ Histone Demethylases**
221 We and others previously reported that ULT1 counteracts the repressive activity of CLF (Carles &
222 Fletcher, 2009; Pu *et al.*, 2013). In order to assess the extent of ULT1 antagonistic effect on CLF, we
223 compared H3K27me3 ChIP-seq datasets for both factors (Shu *et al.*, 2019) and found that CLF targets
224 for repression (thereafter referred to as 'CLF_rep', i.e. genes showing decrease in H3K27me3 amount
225 in *clf* lof) are greatly over-represented among ULT1_derep targets (70,7%, of ULT1_derep are also
226 CLF_rep, p-value<0.001; while only 0,3% of ULT1_derep are SWN_rep, i.e. genes showing decrease in
227 H3K27me3 amount in *swn* lof). In agreement with these results, ULT1_derep are greatly over-
228 represented among CLF_rep (23,6%, of CLF_rep are also ULT1_rep, p-value<0.001; while only 1,6% of
229 SWN_rep are ULT1_derep) (Fig. 2A, Suppl. Table S4). These data indicate that the antagonistic function
230 of ULT1 toward PRC2 is more related to CLF than to SWN.
231 Similarly to ULT1, the RELATIVE OF EARLY FLOWERING 6 (REF6) demethylase can partially
232 counteract CLF activity (Lu *et al.*, 2011) by reducing the amount of H3K27me3 on common genes. We
233 thus wondered whether ULT1 could counteract CLF activity by decreasing H3K27me3 amount through
234 the REF6 pathway (Yan *et al.*, 2018), but found that ULT1_derep and REF6_derep populations share
235 very few common genes (Fig. 2A: 45 genes, corresponding to 1,45% of REF6_derep targets, p-value=
236 $2{,}37.10^{-121}$ for under-representation, and corresponding to 4,91% of ULT1_derep targets, p-value= 0
237 for under-representation). This reveals that ULT1 largely acts in a REF6-independent manner to reduce
238 H3K27me3 levels at target genes. Comparison of H3K27me3 ChIP-seq data between ULT1 and all JmJ
239 HDMTs (analyses in triple mutants for REF6, ELF6 and JMJ12) (Yan *et al.*, 2018), leads to similar
240 conclusions (Supp.l Fig. S9-S11). Moreover, we constitutively expressed *ULT1* in the *ref6-3* mutant
241 background (Fig. 2B) and found that *35S::ULT1* and *35S::ULT1 ref6-3* plants displayed similar

242 developmental defects (small plants with upward curling leaves). We next analysed the expression
243 levels of the MADS-box genes *AG*, *AP3* and *SEP3,* for which H3K27me3 levels are regulated by ULT1,
244 CLF and REF6. We found that these three genes are ectopically expressed to similar levels in *35S::ULT1*
245 and *35S::ULT1 ref6c* (Yan *et al.*, 2018) seedlings (Fig. 2C), demonstrating that ULT1 induces de-
246 repression independently from REF6, even at common target genes. Similarly, *35S::REF6-YFP-HA ult1-*
247 *3* plants do not differ from *35S::REF6-YFP-HA* plants in appearance and both display ectopic expression
248 of *AG*, *AP3* and *SEP3* (Suppl. Fig. S12). This shows that ULT1 is dispensable for ectopic REF6-dependent
249 phenotypes and de-repression of MADS floral genes. Together, these results strongly indicate that
250 ULT1 acts in a REF6-independent manner to decrease H3K27me3 amounts.
251
252 **ULT1 physically interacts with the core PRC2 subunits**
253 To shed light onto the mechanism underlying the ULT1-mediated PRC2 regulation, we
254 investigated potential interactions between ULT1 and PRC2 components in plant cells. To this end, we
255 performed affinity purification coupled with mass spectrometry experiments, conducted on
256 *Arabidopsis thaliana* cell cultures (Antosz *et al.*, 2017) expressing a tagged ULT1 fusion protein (GS-
257 ULT1). The results show that ULT1 copurifies in all three replicates with two core subunits of PRC2:
258 SWN and FIE (Fig. 3A). In addition, we identified an association between ULT1 and ENHANCER OF LIKE
259 HETEROCHROMATIN 1 (EOL1), which interacts physically with CLF and SWN to maintain the H3K27me3
260 mark in plants (Zhou *et al.*, 2017). This data reveals that ULT1 can associate with the PRC2 complex in
261 plant cells, potentially by direct interaction.
262 To verify whether ULT1 interacts with components of PRC2 directly, we performed yeast-two-
263 hybrid (Y2H) experiments (Fig. 3B, C). Indeed, full-length (FL) ULT1 interacts with both FL CLF and SWN_{1-}
264 $_{696}$ a C-terminally truncated version of SWN lacking its SET domain. Yeast growth on selective medium
265 was however much faster with SWN (comparable to that observed for the already reported ULT1-ULT1
266 interaction (Moreau *et al.*, 2016)). $ULT1_{1-193}$, encompassing the N-terminal SAND domain was sufficient
267 for the interactions with CLF and SWN, signifying that the C-terminal Cys-rich domain of ULT1 is not
268 absolutely required. We detected no interaction between ULT1 and the core PRC2 protein FIE by Y2H
269 (data not shown). These results strongly indicate that ULT1 can directly interact with both sporophytic
270 HMTs of PRC2.
271 To test whether ULT1 can directly interact with the PRC2 complexes *in vitro*, we overexpressed in
272 insect cells the catalytic lobes of both $PRC2^{CLF}$ and $PRC2^{SWN}$ containing either the full-length CLF or SWN,
273 FIE and the VEFS domain of EMF2. We based these choices on the known atomic structures of the
274 PRC2 complex in yeast and human (Jiao & Liu, 2015; Justin *et al.*, 2016). The purified PRC2 complexes
275 were used in Strep-tag pull-down assays with pure full-length ULT1 (Fig. 3D, Suppl. Fig. S13). While
276 $PRC2^{SWN}$ bearing a Strep-tag on the FIE subunit could efficiently copurify ULT1 (Fig. 3D, lane 11), in the

277 PRC2^{CLF} co-purification ULT1 was sub-stoichiometric (Fig. 3D, lane 10). The preferential interaction of
278 ULT1 with PRC2^{SWN} was further confirmed by size exclusion chromatography, where ULT1 efficiently
279 formed complex with PRC2^{SWN}, while in complex with PRC2^{CLF}, it co-eluted as sub-stoichiometric (Fig.
280 3E,F).
281
282 **ULT1 enhances PRC2^{SWN} HMT activity and globally functions concordantly to SWN, not CLF, to repress**
283 **target genes**

284 Given the direct interaction of ULT1 with PRC2^{SWN}, we wondered whether this might impact the
285 enzymatic activity of the complex. To address this question, we monitored recombinant PRC2 activity
286 in presence or absence of ULT1, using recombinant nucleosomes as substrate. ULT1 by itself has no
287 enzymatic activity (Fig. 4A,B, lanes 1 to 3). PRC2^{CLF} displays a robust activity which appears rather
288 insensitive to the presence of ULT1 (Fig. 4A,B, lanes 4 to 7). In contrast, PRC2^{SWN}, in this assay, has a
289 modest basal activity which is strongly enhanced in the presence of ULT1 (up to 12-fold when the MBP
290 tag of ULT1 is removed (Fig. 4A,B, lanes 8 to 11). Importantly, while we used a molar excess of ULT1 as
291 compared to PRC2 for this assay, we also performed a titration of ULT1 that showed that its stimulatory
292 effect on PRC2 enzymatic activity can be observed with much lower amount of protein (Suppl. Fig.
293 S14). ULT1 thus seems to function as a strong co-activator of PRC2 with a clear preference for SWN in
294 this assay. Importantly, close examination of the gel also reveals that CLF and SWN are automethylated
295 as it has been described for mammalian PRC2(Lee *et al.*, 2019; Wang *et al.*, 2019) but ULT1 does not
296 appear to be methylated by PRC2. Besides, ULT1 is unable to regulate the mammalian PRC2, which
297 could reflect a plant specific mechanism of action (Suppl. Fig. S15).
298 In agreement with the HMT assays, comparison of target sets and metagenes reveals that ULT1
299 rather functions concordantly to SWN. Indeed, ULT1_rep are greatly under-represented among
300 CLF_rep (4.6%, of CLF_rep are ULT1_rep, p-value<0.001) and greatly over-represented among
301 SWN_rep (36.8%, of SWN_rep are ULT1_rep, p-value<0.001) (Suppl. Fig. S11). Similarly, CLF_rep genes
302 are greatly under-represented among ULT1_rep targets (9.2%, of ULT1_rep are CLF_rep, p-
303 value<0.001), while SWN_rep are greatly over-represented among ULT1_rep (4.9% of ULT1_rep are
304 SWN_rep, p-value for over-representation = $1.74.10^{-12}$). Moreover, average H3K27me3 levels on
305 CLF_rep genes are lower in ULT1 gof lines compared to WT, and they are higher in ULT1 lof lines.
306 Conversely, average K27me3 levels on SWN_rep genes are higher in ULT1 gof lines than in WT, and
307 lower in ULT1 lof plants (Fig. 4C, D). Overall, these data indicate that ULT1 and SWN act in the same
308 direction, while ULT1 and CLF primarily function in opposition, from a genome-wide perspective.
309 Thus, for a large portion of target genes shared between ULT1 and PRC2, ULT1 rather exhibits an anti-
310 PRC2^{CLF} function and a pro-PRC2^{SWN} function.

311

312 **Genetic analyses of *ult prc2* mutants support ULT bivalent interactions with CLF and SWN**

313 We previously found that loss-of-function in ULT1 suppressed *clf* phenotypes, leading to
314 qualification of ULT1 as an antagonist of CLF(Carles & Fletcher, 2009). In order to assess the effect of
315 a full loss of the ULTRAPETALA function on the phenotypes induced by a full loss of PRC2 sporophytic
316 function, we combined mutants for ULT1 and its redundant homologue ULT2, with the two HMTs CLF
317 and SWN. We indeed previously reported that both ULT factors play overlapping roles in Arabidopsis
318 development and gene regulation, with ULT1 playing a major role and ULT2 a minor contribution
319 (Monfared *et al.*, 2013). The triple *clf-28 swn-7 ult1-3* and quadruple *clf-28 swn-7 ult1-3 ult2-2* mutants
320 were indistinguishable from the double *clf-28 swn-7* mutant. They grow as callus-like tissue with
321 random organs that arise in a disorganized phyllotaxy: ectopic roots, somatic embryos, shoot-like
322 structures (Fig. 5A,B, Suppl. Fig. S16,S17). Hence, loss in ULT function does not recover nor further
323 worsens the highly pleotropic defects induced by the loss of PRC2 sporophytic function. These genetic
324 analyses are in agreement with the above ChIP-seq meta-analyses and HMT assays, which indicate
325 both ULT1 antagonism toward CLF and cooperativity toward SWN.

326

327 ***FLC* and *WUS* genes are key nodes for ULT1-PRC2 cooperative regulation of developmental**
328 **transitions**

329 The phenotypes of ULT1 lof (late flowering) and ULT1 gof (early flowering) lines consistently
330 provide evidence that ULT1 functions as a promoter of the reproductive transition (Carles *et al.*, 2005);
331 Carles & Fletcher, 2009) (Suppl. Fig. S18). Moreover, the central repressor of flowering *FLC*, master
332 target gene for regulation by PRC2, also stands out as a target gene repressed by ULT1 (Tables S1, S3,
333 Suppl. Fig. S18C, Fig. 5C). By generating a *ult1flc* double mutant, in which *flc* lof suppresses *ult1*
334 flowering delay, we revealed that *FLC* is indeed responsible for the late flowering transition in *ult1*
335 mutant (Fig. 5D, E).

336 Because *FLC* is also a target of SWN (Shu *et al.*, 2020), we investigated the flowering phenotypes of
337 triple mutants lacking both ULT and SWN functions, and could not detect significant difference to the
338 *ult* lof double mutant (Fig. 5F). Moreover, *FLC* expression is upregulated in both *ult1 ult2* double and
339 *ult1 ult2 swn* triple mutants, and brought to a yet higher level in the triple mutant (Fig. 5G). This
340 observation is consistent with a cooperative role for the two factors. Strikingly, triple mutants lacking
341 both ULT and CLF functions were dramatically delayed in flowering (Fig. 5H,I), with a strong
342 upregulation of *FLC* expression (Fig. 5J). We interpret this as the manifestation of ULT role in enhancing
343 SWN function, which is normally partly masked in the presence of CLF (Fig. 5K), likely because CLF can
344 replace SWN. Furthermore, the weaker late flowering time phenotypes and *FLC* de-repression in *swn*
345 *ult1 ult2* triple mutant as compared to the *clf ult1 ult2* triple mutant (Fig. 5F) indicates that CLF may

346 compensate better for the absence of SWN than SWN does compensate for the absence of CLF. Hence,
347 the *clf ult1 ult2* plants likely reveal how a *clf swn* double mutant would flower if it could establish
348 correct meristematic structures and body plan. These results also reveal a synergistic interaction
349 between ULT and CLF for *FLC* regulation.

350 The production of supernumerary floral organs in *ult1* mutant lines was previously attributed to
351 an expansion in the expression domain of the *WUS* meristem regulator(Carles *et al.*, 2004, 2005). We
352 found that flowers of triple mutants lacking both ULT and SWN functions produce the same number
353 of organs, for each whorl, as do flowers of double mutants lacking the ULT function only (Suppl. Fig.
354 S19A,B). Differently, triple mutants lacking both ULT and CLF functions produce flowers with more
355 floral organs than *ult1 ult2* double mutants (Suppl. Fig. S19C,D). This indicates a synergistic interaction
356 between ULT and CLF, which could be due to their separate functions (ULT rather being a cofactor of
357 SWN) in repressing *WUS*. Moreover, another pathway could be considered for ULT, independent of
358 PRC2, involving a direct interaction with the UIF1 transcription factor which has a repressive function
359 on *WUS* expression (Suppl. Fig. S19E)(Moreau *et al.*, 2016).
360
361 The similar phenotypes of *ult* and *ult swn* lines, both for flowering time and flower organ numbers,
362 testify for the cooperativity of ULT and SWN. Our genetic analyses, through the two case examples of
363 *FLC* and *WUS*, thus support the model along which ULT1 helps SWN to repress genes by stimulating
364 the H3K27me3 histone methyltransferase activity of the $PRC2^{SWN}$ complex; but in the absence of
365 functional SWN, $PRC2^{CLF}$ efficiently compensates for H3K27me3 deposition. ULT1 thus likely stands as
366 a moderator of PRC2 function via enhancement of SWN activity.
367
368
369 **Discussion**

370 In this study, we report for the first time the genome-wide effect of the ULT1 protein on the
371 abundance of the PcG/PRC2-mediated H3K27me3 and the trxG-mediated H3K4me3 marks, along with
372 its effect on the transcriptome. In order to avoid the consequences of developmental defects but
373 rather observe their epigenetic origin, we ran ChIP-seq and RNA-seq analyses on young seedling tissue
374 (8do). This allowed to detect significant populations of genes differentially marked with H3K27me3,
375 and slighter effects on H3K4me3 and on gene expression levels. This likely testifies that ULT1 functions
376 post-embryonically as a regulator of PcG/PRC2 activity , rather than as a regulator of trxG activity.

377 Using AP-MS, Y2H and *in vitro* assays, we demonstrated that ULT1 directly interacts with CLF and
378 SWN within the PRC2 complex. Interaction tests of ULT1 with SWN resulted in faster yeast growth and
379 greater *in vitro* enrichment compared to CLF. By coupling these analyses with HMT assays, we
380 uncovered a novel function for the ULT1 protein as a direct $PRC2^{SWN}$ activator. These results also

381 highlighted an important difference between the PRC2 complexes carrying either the CLF or the SWN
382 enzyme ($PRC2^{CLF}$ vs $PRC2^{SWN}$). Using recombinant nucleosomes as substrate, the basal activity of
383 $PRC2^{SWN}$ appears to be lower than that of $PRC2^{CLF}$. Importantly, under these experimental conditions,
384 ULT1 markedly enhances the enzymatic activity of $PRC2^{SWN}$ activity, while it has a limited or negligible
385 effect on the activity of $PRC2^{CLF}$. This is coherent with observations made using single and double
386 mutants affected in CLF and SWN (Chanvivattana *et al.*, 2004). Indeed, while the sporophytic
387 phenotypes of *clf* null mutants are severe (dwarf plants with upward curled leaves and early flowering),
388 those of *swn* null mutants are very subtle (no visible morphological defect, only a slight delay flowering
389 transition). However, the absence of both sporophytic HMTs has dramatic effects, double *clfswn* null
390 mutants being unable to establish a proper plant body plan. This indicates that, while the $PRC2^{CLF}$
391 complex might be more efficient at repressing common target genes than the $PRC2^{SWN}$ complex, SWN
392 can effectively exert an activity similar to that of CLF in its absence. The two corresponding functions
393 are therefore paralogous with an unequal redundancy. Mutual complementation tests support that
394 CLF and SWN are not interchangeable; indeed while *clf* plants are complemented by a *35S::CLF*
395 transgene, they are not complemented by a *35S::SWN* transgene (Chanvivattana *et al.*, 2004).
396 Interestingly, this is unlikely to be due to different genes bound by CLF or SWN, since they share a large
397 majority of targets, as indicated by ChIP-seq profiling (Shu *et al.*, 2019). Based on CLF/SWN overlapping
398 target genes and on our results, we propose that the difference in gene repression efficiency between
399 $PRC2^{CLF}$ and $PRC2^{SWN}$ is likely due to differences in the nature of the two proteins. It could reside in a
400 differential enzymatic activity at many common targets, that may be dependent on ULT1 presence, as
401 supported by our *in vitro* HMT activity tests. Nevertheless, an additional and non-exclusive regulatory
402 layer, involving differential binding specificity or affinity to targets, could also explain the differential
403 *clf* vs *swn* defects observed in plants. Further investigations, assessing e.g. the relative affinities of
404 $PRC2^{CLF}$ and $PRC2^{SWN}$ complexes for nucleosomes and chromatin targets, both biochemically and *in*
405 *planta* will be needed to elucidate the molecular details of this mechanism.
406 While it would be tempting to compare $PRC2^{EZH1}$/$PRC2^{EZH2}$ to $PRC2^{SWN}$/$PRC2^{CLF}$ according to their
407 respective contribution to H3K27me3 global levels ($PRC2^{EZH1}$ and $PRC2^{SWN}$ being on the lower side),
408 their regulation seems to obey different rules. Indeed, in addition to its lower basal activity, $PRC2^{EZH1}$
409 tends to respond less efficiently to activating cues such as H3K27me3-mediated allosteric activation
410 (Lee *et al.*, 2019). In contrast, we showed that $PRC2^{SWN}$ responds better to ULT1-mediated enzymatic
411 activation. Taken together, these results prompt for further mechanistic and structural investigation
412 into $PRC2^{SWN}$ and $PRC2^{CLF}$ regulation.
413
414 In plants, the ULT function (ULT1, combined to its functional homologue ULT2 (Carles *et al.*, 2005))
415 is likely responsible for the increase of $PRC2^{SWN}$ activity to the level of $PRC2^{CLF}$ activity. Indeed, we

416 previously reported that the ULT1 and ULT2 proteins are involved in common key developmental
417 processes such as flowering time and organogenesis, through the regulation of inflorescence meristem
418 activity (Carles *et al.*, 2005); (Monfared *et al.*, 2013). Interestingly, the weak *emf2 vrn2* double mutant,
419 impaired in two SU(Z)12 alternative PRC2 subunits, displays a late flowering phenotype and additional
420 floral organs (Muller-Xing *et al.*, 2014), phenotypes very reminiscent of *ult* mutants. This strongly
421 supports that the severe delay in reproductive transition displayed by the *clf ult1 ult2* triple mutant
422 likely reveals the hidden, joined function of the two alternative CLF and SWN HMTs for *FLC* repression.
423 This function cannot be seen in a *clf swn* double mutant, as it no longer develops as a real plant but a
424 cluster of randomly differentiated cells and tissues. The same is true for the extra flower organs
425 observed in the *clf ult1 ult2* triple mutant, which are significantly more numerous than in *a ult1 ult2*
426 double mutant. Our interpretation of these results is that when CLF is present, repression of *FLC* or
427 *WUS* still occurs, but if CLF is missing, the relay is taken to some extent by SWN, whose function is
428 enhanced by ULT. The *FLC* and *WUS* target loci thereby provides demonstrative examples for the
429 developmental effect of ULT as cofactor of PRC2, which moreover discriminates between CLF and
430 SWN. In addition, meta-analyses of H3K27me3 ChIP-seq data obtained for ULT1, CLF and SWN, allow
431 to broaden this statement to more genes. Moreover, these meta-analyses reveal two distinct sets of
432 target populations: one that is repressed by CLF, on which ULT1 rather functions as an anti-PRC2, and
433 another one targeted by SWN, on which ULT1 rather exerts a pro-PRC2 function. This discrepancy
434 could be explained by ULT1 role as enhancer of SWN, which may in some way compete with the more
435 efficient activity of CLF.
436
437 Our dataset indicates that the ULT1 counter-PRC2 role is independent from the JmJ H3K27me3
438 demethylases. A possibility is that ULT1 could prevent PRC2 function via direct interaction, in a specific
439 context. Another, non-exclusive hypothesis is that ULT1 could prevent methylation of *de novo*
440 synthesized Histone 3 proteins in dividing stem cells, where it is preferentially expressed (Carles *et al.*,
441 2005). This may occur independently from a physical interaction with PRC2, but rather via DNA binding
442 of transcription factors (TFs) that evict PRC2 from target genes, as previously reported for AG (Sun *et*
443 *al.*, 2014). ULT1 has been reported to directly interact with TFs, members of the MYB and GARP families
444 in flower meristems in particular (Pires *et al.*, 2014; Moreau *et al.*, 2016); however it is yet unknown
445 whether these TFs can oppose the deposition of H3K27 methylation. Consistent as well with a
446 competition scenario against the propagation of the H3K27me3 mark, the ULT1 IP-MS dataset includes
447 potential ULT1 physical partners that either physically or genetically interact with PRC2, or are involved
448 in DNA replication processes: ENHANCER OF LHP1 (EOL1), EARLY IN SHORT DAYS 7 (ESD7) and
449 INCURVATA 2 (ICU2) (Barrero *et al.*, 2007; del Olmo *et al.*, 2016; Zhou *et al.*, 2017; Jiang & Berger,

450 2017; Godwin & Farrona, 2022). ULT1 may therefore prevent histone mark maintenance during cell
451 division, through interaction with these components.
452
453 Overall, this study demonstrates that ULT1 acts as a developmental switch that can either
454 counteract or stimulate PRC2 repressive function on distinct sets of target genes. Moreover, our
455 integrative approach shows that ULT1 can enhance the activity of PRC2 both *in vitro* and *in vivo*. This
456 is the first evidence of a trxG protein directly interacting with PRC2 and enhancing its activity.
457 Interestingly, in animals, PRC2 can also methylate non-histone proteins, including its cofactor Jumonji
458 and AT-Rich Interaction Domain Containing 2 (Jarid2) and this methylation was shown to be important
459 to promote PRC2 activity (Sanulli *et al.*, 2015). In contrast, our results indicate that ULT1 can stimulate
460 PRC2 activity despite not being methylated, which indicates a novel mechanism for PRC2 stimulation,
461 yet to be elucidated. Furthermore, our work provides insights into the redundant and distinct functions
462 of CLF and SWN (Shu *et al.*, 2020), both at the molecular and developmental levels, and pinpoints ULT1
463 as a key factor influencing the differing roles of CLF and SWN at cell fate transition genes. We indeed
464 report the first HMT activity tests for SWN and show that $PRC2^{CLF}$ and $PRC2^{SWN}$ complexes have
465 different catalytic efficiencies. This is in accordance with phenotypic studies revealing that, while
466 mutation in *clf* leads to strong phenotypes, mutation in *swn* is indistinguishable from wild type plants
467 (Chanvivattana *et al.*, 2004).
468 More broadly, we revealed a molecular mechanism that lies at the crossroads of antagonism and
469 collaboration between PcG/PRC2 and trxG.

470 **Conclusions**

471 Using an integrative approach combining developmental genetics, genomics and biochemistry,
472 we uncovered a unique and novel function that regulates PRC2 HMT activity in plants. We found that
473 ULT1 counteracts deposition of the repressive H3K27me3 mark at hundreds of developmental genes
474 independently of histone demethylases. Additionally, ULT1 promotes PRC2 activity at hundreds of
475 other developmental genes. This pro-PRC2 activity is linked to its direct interaction with the SWN HMT
476 and the enzymatic activation of $PRC2^{SWN}$.

477 Together, our discoveries reveal a mechanism by which developmental transitions at the shoot
478 apex are driven. First, they decouple inhibition of methylation from active demethylation, providing
479 insights into how the switch from H3K27me3-repressed to active genes operates in meristematic
480 regions. Second, they provide a novel mechanism of PRC2 activity enhancement, in which ULT1, via
481 direct interaction with $PRC2^{SWN}$, raises deposition of H3K27me3 on nucleosomes, and seems to do this
482 through a mechanism different from that of the Jarid2 PRC2 co-factor in animals.

483

484

485 **Online Methods**

486

487 ***Arabidopsis mutants and transgenic lines***

488 The *Arabidopsis thaliana* (Arabidopsis) lines used in this study were in the Columbia-0 (Col-0) or
489 Landsberg erecta (Ler) ecotype backgrounds. The mutant lines *ult1-2*, *ult1-3* (SALK_074642C,
490 introgressed or not in Ler), *ult2-2* and *ref6-3* were previously described (Carles *et al.*, 2005; Lu *et al.*,
491 2011; Monfared *et al.*, 2013). The mutant lines *clf-28* (Salk_139371)(Lopez-Vernaza *et al.*, 2012) and
492 *swn-7* (Salk_109121), also known as *swn-4* (Wang *et al.*, 2006) are in the Col-0 background. The *clf-*
493 *28/+ swn-7* line was kindly provided by Daniel Schubert and used to cross to the double mutant *ult1-3*
494 *ult2-2* in Col-0 (Monfared *et al.*, 2013) in order to obtain the quadruple mutant *clf-28 swn-7 ult1-3 ult2-*
495 *2*.

496 The constructs used for transgenic lines were introduced in Arabidopsis plants by Floral dip
497 agrobacterium-mediated transformation. *Agrobacterium tumefaciens*, strain C58C1pMP90, carrying
498 the *p35S::ULT1* (Carles & Fletcher, 2009) or the p*35S::REF6-YFP-HA*, (Lu *et al.*, 2011) construct were
499 grown overnight at 28°C in 2ml of selective LB medium and 1 ml of this culture was then spread on
500 YEB medium supplemented with antibiotics and grown at 28°C during 72hr. Grown colonies were
501 dissolved in 50ml LB and grown at 28°C during 2hr, before being pelleted and resuspended with 200ml
502 of a 5% sucrose solution containing 0.01% of Silwet L-77. Inflorescences of *ref6-3* or *ult1-3* mutants or
503 Col-0 WT control plants were dipped into this bacterial culture during 10s. The dipped plant (T0) were

504 grown within a controlled environment until their seeds were fully mature. T1 generation seeds were
505 collected from T0 plants and further selected for antibiotic resistance on MS selective medium.
506 When cultivated *in vitro*, seeds were sterilized (70% ethanol solution-5min and 95% ethanol solution-
507 5min, dried on Whatman paper), sown on ½ MS medium supplemented with 1% sucrose, and then
508 stratified for 3 days at 4°C. Seeds were further germinated within a controlled environment chamber
509 at 20°C with 16hr light/8hr dark photoperiod and under 65% humidity.
510 When directly sown on soil, seeds were stratified for 3 days at 4°C, and then transferred in a controlled
511 environment chamber at 20°C with 16hr light/ 8hr dark photoperiod and under 65% humidity.
512
513 ***Chromatin immunoprecipitation followed by deep sequencing (ChIP-seq)***
514 ChIP-seq was performed in 8 day old seedlings of Ler, *ult1-2*, *ult1-3*, *35S::ULT1*, Col-0 and *ref6-3* grown
515 in long day (LD) conditions of 16 h light (18 degrees) and 8 h darkness (16 degrees) on Murashige and
516 Skoog medium (Sigma-Aldrich, Lyon, France) supplemented with 0.3% sucrose in growth cabinets
517 (Percival, Percival Scientific Incorporated, provided by CLF Plant Climatics, Emersacker, Germany) .
518 ChIP-seq experiments for H3K27me3 and H3K4me3 marks were conducted on immuno-precipitates
519 prepared from the same chromatin extracts, following the protocol described in (Engelhorn *et al.*,
520 2017b). Two independent biological replicates were used, with three technical replicates pooled for
521 sequencing in each case.
522 Antibodies and quality control were described previously (Engelhorn *et al.*, 2017a). Sequencing was
523 performed as described for replicate 2 (Engelhorn *et al.*, 2017a).
524 Read mapping, processing and determination of differentially marked regions was performed as
525 described in (Engelhorn *et al.*, 2017b). For replicate 2 of H3K27me3 in *ult1-2* and *ult1-3*, read numbers
526 were so high that peaks displayed saturation. Therefore, for the quantitative comparison, duplicates
527 were not removed. Only regions differentially marked in both replicates were considered for further
528 analysis.
529 For comparisons of H3K27me3 patterns in PcG/trxG mutants *clf, swn* and *elf6-3 ref6C jmj13G*, raw data
530 from ChIP-seq experiments performed in (Shu *et al.*, 2019) and (Yan *et al.*, 2018) was downloaded
531 from GeoAccession GSE108960 and GSE106942 and analysed using the same parameters employed
532 for the libraries generated in this study. For *elf6-3 ref6C jmj13G* no input was available, thus an E-value
533 cutoff of 100 was chosen in the SICER analysis (Zang *et al.*, 2009).
534 Significant over- and under-enrichment for comparisons of differentially histone marking target gene
535 overlaps was calculated by hypergeometric testing in R (Version 4.1.2) using the phyper function and
536 all WT Ler H3K27me3 targets as total number of targets.
537 Heatmaps and metagene plots were produced with deeptools (v3.5.1) (Ramírez *et al.*, 2016). Genomic
538 coverage screenshots were taken with Integrated Genome Browser (v10.0.0) (Freese *et al.*, 2016).

539

540 ***ChIP-qPCR***

541 For ChIP-qPCR independent IPs were performed on the same material as employed for ChIP-seq plus
542 a third replicate. The same protocol was followed for the ChIP-seq IPs with the exception of the
543 sonication. In order to obtain longer fragments for qPCR, sonication was performed for 10 min with 15
544 sec on 1 min off cycles in a Bioruptor machine (Agilent) filled with ice-cold water at strength H. Nuclear
545 extracts were diluted 1:10 and 2 ul of this dilution were used as template in a total reaction volume of
546 10 ul using SsoFast Eva Green Supermix with primers at 0.4 uM (primer sequences are provided in
547 Table S5). Technical triplicates were performed for each sample analysed. The quantitative PCR
548 reaction was performed on a Biorad CFX Connect machine.

549

550 ***RNA extraction followed by deep sequencing (RNA-seq)***

551 RNA-extraction, sequencing and analyses were performed on RNA prepared from the same tissues as
552 those used for chromatin preparations as well as a third replicate, as described in (Engelhorn *et al.*,
553 2017a) and (Engelhorn *et al.*, 2017b), using TopHat v2.1.1, cuffdiff v2.2.1. For comparison of single
554 gene counts, Fragments per kilobase per million read (FPKM) values were generated using cuffnorm
555 v2.2.1 with library-norm-method geometric (Trapnell *et al.*, 2012). For ULT1 gof, an independent
556 insertion was chosen as the third replicate. All of these *35S::ULT1* replicates show ULT1 over-
557 expression in RNA-seq (ULT1 FPKM: 685.3 809.8 and 512.4 in rep1-3; Ler FPKM: 16.8, 10.2 and 10.3 in
558 rep1-3). Volcano plots were generated with ggplot2 (v3.4.4) [https://ggplot2.tidyverse.org].

559

560 ***Gene Ontology analyses***

561 GO enrichment analyses were performed in different gene sets using ShinyGO tool v0.8 (Ge *et al.*,
562 2020). We used the WT Ler marked genes for either H3K27me3 or H3K4me3 as a background. Terms
563 were sorted by increasing -10log(FDR).

564

565 ***Western-blots on marks***

566 Nuclear extracts were extracted from 3 to 4.5 g of 8 or 13 days old seedlings according to the protocol
567 described in (Huq *et al.*, 2003) with minor modifications: in Nuclear Grinding Buffer (NGB,
568 iodoacetamide, PMSF, aprotinin, pepstatin and leupeptin were replaced by one tablet of Thermo
569 ScientificTM Pierce Protease Inhibitor. Nuclear pellets were resuspended in NGB with SDS at a final
570 concentration of 0.2%. The nuclear extracts were sonicated and Laemli 5X buffer was added. Samples
571 were loaded on a 15% polyacrylamide gel and transferred onto a nitrocellulose membrane using
572 InvitrogenTM iBlot 2 Dry Blotting System. The primary antibodies were Abcam ab1791 (H3), Milipore
573 07-419 (H3K27me3), Abcam ab24264 (H3K27me2), Invitrogen 491012 (H3K27me1) The secondary

574 antibody was the HRP-AffiniPure Goat Anti-Rabbit IgG (H+L) (JIR 111-035-003). Detection was
575 performed using BioRad Clarity™ ECL substrate. The membranes were incubated with Thermo
576 Scientific™ Restore™ PLUS Western Blot Stripping Buffer during one minute with and washed with T-
577 TBS for stripping before re-probing.
578
579 ***Immuno-fluorescence and DAPI staining of nuclei***
580 Eight-day-old plants were harvested and fixed for 30 minutes in 4% formaldehyde in PME buffer (50
581 mM PIPES, 5 mM MgSO4, 1 mM EGTA, pH 6.5). Samples were washed and transferred to a Petri dish,
582 chopped in enzyme mix (1% cellulase, 0.5% pectolyase, and 1% cytohelicase) and incubated 30 minutes
583 at RT. Suspension was filtered through nylon mesh (pore size 30 µm) and spread on poly-lysine coated
584 slides, 20µL of 1% lipsol in PME was added on the slide and spread, then 20µL of 4% paraformaldehyde
585 in PME was added and spread, and the slides left to air dry. Slides were incubated with 0.5% Triton X-
586 100 in 1X PBS for 15 minutes at RT in a moist chamber, washed in 1X PBS, and incubated overnight at
587 4°C with 1:400 of H3K27me3 (C154110069, Diagenode, batch A1818P) in 3% BSA, 0.05% Tween-20 in
588 1X PBS then washed and incubated 3 hours at RT with 1:1000 of Alexa Fluor™ 488 (A-11070) diluted in
589 3% BSA, 0.05% Tween-20 in 1X PBS. Nuclei were imaged with a Zeiss LSM 800 AiryScan confocal
590 microscope using a 63X objective.
591
592 ***Analysis of nuclear parameters***
593 Seeds of WT, *clf* mutant and ULT1 overexpressing lines were surface sterilized (75% ethanol/5 min and
594 then 96% ethanol/5 min) and plated on half-strength agar Murashige and Skoog medium (½ MS
595 medium) containing 1% sucrose. After 2 days of stratification (4°C/dark) plates were grown in a growth
596 chamber under long day conditions (16h Light / 8h dark). To analyse nuclear parameters, we fixed
597 cotyledons from 9-day-old or 14-days old seedlings as described previously (Desset *et al.*, 2018).
598 Cotyledon tissue was stained overnight with gentle shaking with Hoechst (Hoechst 33, 258 at 1 µg/ml
599 final). under gentle shaking. After extensive washing in PBS, cotyledons were mounted in PBS:glycerol
600 (20:80) and wide-field images of the cotyledon epidermis were acquired with a Leica DM6000 B
601 microscope equipped with an Optigrid® system to perform structured illumination microscopy with a
602 63X/1.4–0.6 oil-immersion objective. Using the NucleusJ 2.0 autocrop option (Dubos *et al.*, 2020). 3D
603 images containing one single nucleus were obtained. Nucleus and chromocenters were segmented
604 using a deep-learning model for chromocenters and one for nuclei (detailed in Machelova, TPJ, in
605 press) in the deep learning Python package biom3D (Mougeot *et al.*, 2024). All segmentation
606 predictions were verified by the user after overlay with the respective raw image and obviously
607 aberrant predictions discarded. Quantitative parameters of the nuclear and the chromocenter volume
608 were subsequently extracted from the resulting segmentations to calculate the volume RHF (relative

609 heterochromatin fraction) as the chromocenter volume divided by the nuclear volume. Two
610 independent experiments with similar results were carried out.
611
612 ***RT-qPCR***
613 To quantifiy transcript levels, total RNAs were isolated from 8-day-old seedlings using the RNeasy™
614 plant mini kit (Qiagen). Reverse transcription was then performed on 1 to 2 µg of total RNA using the
615 Master Mix Super Script™ IV Vilo™ (ThermoFisher Scientific). Quantitative PCR reactions were
616 performed with the Power SYBR™ Green master mix (ThermoFisher Scientific), with forward and
617 reverse primers each at 0.2 µM, in a total reaction volume of 10 µl. The list of primers is provided in
618 primer sequences in Table S5. Technical triplicates were performed for each sample analysed. The
619 quantitative PCR reaction was performed on a Biorad CFX Connect machine. The results were analysed
620 using the REST spreadsheet (Pfaffl *et al.*, 2002).
621
622 ***Affinity Purification followed by Mass Spectrometry (AP-MS)***
623 For affinity-purification coupled to mass spectrometry (AP-MS) experiments, ULT1 coding sequence
624 was cloned in the pCambia2300-5´GStag- polyA vector, at the KpnI and EcoRI sites, to generate a GS
625 tag-ULT1 fusion (tag in the N-terminus end of ULT1). Affinity purification was performed as described
626 in (Pfab *et al.*, 2017). Briefly, IgG-coupled magnetic beads were used to purify under mild conditions
627 the GS-tagged ULT1 and its potential interactors from *A. thaliana* suspension cultured cells. The
628 samples were then submitted to mass spectrometry to identify the interactors. The experiment was
629 performed in triplicates. IDs corresponding to contaminating proteins copurifying non-specifically
630 independent of the used bait protein in similar AP-MS experiments were filtered out (Van Leene *et al.*,
631 2015).
632
633 ***Yeast-two-hybrid (Y2H) assays***
634 For binary interaction tests, the candidate partners were expressed as Gal4DNA-BD (BD: binding
635 domain) or Gal4AD (AD: activation domain) fusion proteins. For this, all cDNAs were cloned into pGAD-
636 T7 and pGKB-T7 vectors (Clontech) and were transformed into yeast strains AH109 and Y187,
637 respectively, for mating according to the manufacturer. ULT1 and UIF1 full-length and truncated
638 versions were previously described in (Moreau *et al.*, 2016) and CLF and SWN clones were previously
639 described in (Chanvivattana *et al.*, 2004). A shortened version of SWN, SWNΔSET (SWN_{1-696}) in which
640 the histone methyl transferase SET domain is absent, was used in these experiments. ULT1 and CLF or
641 SWN-transformed yeast strains were mated and the resulting diploids were selected for the presence
642 of both plasmids with medium lacking Leu and Trp (−LW). Selected yeast strains (containing both a
643 pGADT7 vector and a pGBKT7 vector) were resuspended in water at two densities, OD600nm=10 and

644 OD_{600nm}=1. Drops of 5µL of resuspended yeast were then dotted on −LW or –LWAH medium (lacking
645 Leu, Tryp, His and Ade) on which only the diploids presenting protein interactions can grow. The plates
646 were incubated at 30°C for 3 to 5 days and yeast growth was monitored every day.
647
648 ***Production and purification of recombinant PRC2 and ULT1***
649 To produce the catalytic lobes of the two PRC2 complexes in the baculovirus expression system, His-
650 tagged full-length CLF and SWN were respectively cloned into the Multibac acceptor vector pFL
651 (Fitzgerald *et al.*, 2006). Strep-tagged full-length FIE and C-terminally Flag-tagged EMF2 VEFS domain
652 (residues 468-631) were respectively cloned into the donor vectors pUCDM and pIDK. The two donor
653 vectors were recombined with the acceptor pFL carrying either CLF or SWN using Cre-recombination,
654 generating two Multibac plasmids coding for either trimeric $PRC2^{SWN}$ or PRC^{CLF}. The PRC2 plasmids
655 were inserted into the bacmids DNA and used to transfect Sf21 insect cells, resulting in the production
656 PRC2-producing baculoviruses. The complexes were expressed by infecting High Five cells with the
657 baculoviruses at 27°C for 72 hours. Following cell disruption, supernatants containing soluble
658 complexes were incubate for 2 hours with Ni^{2+}-Chelating Sepharose (Cytiva). The resin was washed
659 with a buffer containing 25 mM HEPES, pH 7.8, 150 mM NaCl, 1 mM TCEP, 2 mM $MgCl_2$, and 10 mM
660 imidazole, followed by a high-salt buffer wash with 1 M NaCl. The bound complex was eluted by
661 increasing the imidazole concentration to 300 mM. To obtain a stoichiometric complex, the eluted
662 complex was further purified by Strep-Tactin XT resin (IBA) and size exclusion chromatography on a
663 Superdex 200 Increase (Cytiva) in a buffer containing 25 mM HEPES pH 7.8, 150 mM NaCl, 1 mM TCEP,
664 2 mM MgCl2 and 2% glycerol.
665 Full-length ULT1 was expressed in E. coli Rosetta 2 cells (Novagen) from the pETM41 vector (EMBL,
666 Gunter Stier) as His-MBP-tag fusion. Before induction, the growth medium was supplemented with
667 1mM $ZnSO_4$. The protein was first purified on Amylose resin (NEB) and the aggregated species were
668 eliminated by gel filtration on Superdex 200 Increase (Cytiva) in a buffer containing 25 mM HEPES pH
669 7.8, 300 mM NaCl, and 10 mM DTT. After the His-tag removal by TEV protease the protein was further
670 purified on a Heparin HiTrap column (Cytiva) and another gel filtration on Superdex 200 Increase
671 (Cytiva).
672
673 ***Pull-down assays***
674 The purified PRC2 complexes ($PRC2^{CLF}$ and $PRC2^{SWN}$) and untagged ULT1 protein were prepared in a
675 buffer containing 25 mM HEPES, pH 7.8, 100 mM NaCl, 1 mM TCEP, 2 mM $MgCl_2$ and 2% glycerol and
676 mixed in a molar ratio of 1:3, respectively. The mixture was incubated for 30 minutes before being
677 loaded onto Strep-Tactin XT (IBA) resin columns. The resin was extensively washed with a buffer

678 containing 25 mM HEPES pH 7.8, 100 mM NaCl, 1 mM TCEP, 2% glycerol, and 2 mM $MgCl_2$, and the
679 bound proteins were eluted by adding 50 mM D-Biotin and analyzed by 15% SDS-PAGE.
680
681 ***HMT activity assays***
682 HMT assays were performed with 1.5ug of PRC2-CLF or PCR2-SWN alone or in presence of 0.75ug of
683 MBP or MPB-ULT1 or ULT1 incubated at 30°c for 30min in the reaction buffer containing 50 mM Tris-
684 HCl (pH 8.5), 5 mM MgCl2, 4 mM DTT, and 1 µM 3H-labeled SAM (Amersham Pharmacia Biotech).
685 0.75ug of recombinant histone oligo-nucleosomes were used as substrate. The total volume of the
686 reaction mixture was adjusted to 25 µl. The reaction was stopped by addition of SDS sample buffer
687 and boiled for 5mn at 95°c. The samples were then fractionated by 15% SDS-PAGE, transferred to a
688 PVDF membrane, and stained with Coomassie. The membranes were exposed overnight on a
689 phosphorimager screen and revealed on an imager typhoon (Cytiva).
690
691 ***Obtention of the* clf swn ult1 ult2 *multiple mutants***
692 Multiple mutants were obtained from an initial cross between *clf-28/+ swn-7* and *ult1-3 ult2-2* lines,
693 both in the Col-0 ecotype.
694 *clf-28 swn-7 ult1-3* triple mutant
695 The progeny of a *clf-28 swn-7+/- ult1-3* line was grown on ½ MS medium (1% sucrose) for 15 days at
696 20°C in long days (16hr light/8hr dark). Out of 150 seedlings, 35 displayed a *clf swn* double mutant
697 phenotype and were confirmed to be homozygous for the *swn-7* mutation by genotyping (see primer
698 sequences in Table S5).
699 *clf-28 swn-7 ult1-3 ult2-2* quadruple mutant
700 Due to genetic linkage of approx. 2-4 cM between the *CLF* and *ULT2* loci, we attempted to obtain the
701 *clf-28 swn-7 ult1-3 ult2-2* quadruple mutant first using the CRISPR Cas9 method to create an *ult2*
702 mutant, which turned unsuccessful, second by a high throughput screen through a population
703 obtained by genetic crossing. For this, we screened through the progeny of a *clf-28/+ swn-7 ult1-3 ult2-*
704 *2/+* plant. 550 seeds were grown on soil and genotyped for *ult2-2* and *clf-28/+* mutations (primer
705 sequences provided in Table S5). One plant displayed the expected genotype *clf-28/+ swn-7 ult1-3*
706 *ult2-2*. Phenotypic observations on the progeny of this plant were carried out *in vitro*.
707
708 ***Phenotypic analyses of the* clf swn ult1 *triple and* clf swn ult1 ult2 *quadruple mutants***
709 200 seeds were sown for each the following genotypes, and grown on ½ MS (1% sucrose), at 20°C (16hr
710 light/8hr dark; 65% humidity): *clf-28 swn-7+/- ult1-3* and *clf-28+/- swn-7 ult1-3 ult2-2* as well as the
711 control lines *clf-28+/- swn-7* and *clf-28 swn-7*. After 15 days of growth, *clf*-like seedlings were counted
712 under the binocular microscope SZX12 and genotyped for *clf-28*, *swn-7* and *ult2-2* mutations.

713

714 ***Imaging by multifocal microscope and Environmental Scanning Electron Microscope (SEM)***

715 We followed the evolution of the *clf*-like phenotypes after two months of *in vitro* growth, and
716 transplanted the corresponding mutants onto fresh ½ MS medium (1% sucrose) after 1 month. Pictures
717 of these mutants were taken with the VHX-5000 Keyence numeric multifocal microscope as well as
718 with an environmental SEM. SEM experiments were performed at the Electron Microscopy facility of
719 the ICMG Nanobio-Chemistry Platform (Grenoble, France). Untreated tissues were directly placed in
720 the microscope chamber. Care was taken to maintain some humidity during the pressure decrease in
721 the chamber in order to prevent tissue drying. Secondary electron images were recorded with a
722 Quanta FEG 250 (FEI) microscope while maintaining the tissue at 2◦C, under a pressure of 500 Pa and
723 a 70% relative humidity. The accelerating voltage was 14 kV and the image magnification ranged from
724 100 to 800x.

725

726 ***Flowering time and Floral organ counting***

727 The flowering times were measured by the leaf counts at bolting. For floral organ counting the first 10
728 open flowers from 10 plants were counted from each genotype. A Wilcox statistical test was
729 performed on experimental data.

730

731

732

733 **Acknowledgements**

734 We thank Evelyna Damyanova for help with technical realization of the ChIP used in qPCR, Enora Fremy
735 for preliminary Y2H assays, Renaud Dumas and Catarina Da Silva for help in designing ULT1 protein
736 production strategies, François Parcy for discussions and infrastructure share, Stéphane Ravanel for
737 preliminary HMT assays, Franziska Turck for sharing *clf/swn* ChIP-seq data prior to publication and
738 Christine Lancelon-Pin for SEM manipulations (at Cermav Grenoble), and the iGReD CLIC microscopy
739 facility for image acquisition.

740

741

742 **Author contributions**

743 Conceptualization, C.C.C. and J.E.; methodology, C.C.C, J.E., G.V., J-B. I., J. K. and V.G.; formal analysis,
744 C.C.C., J.E., G.V., J.K., V.G, R. M. and L.T.; investigation, J.E., V.G., C.T., J-B. I., H.L., J.K., A.P., M.L.M. and
745 C.C.C.; writing – original draft, C.C.C.; writing – review & editing, C.C.C. with help of J.E., J.K. V.G, G.V.,
746 L.T.; funding acquisition for this specific study, C.C.C. and J.K.

Declaration of interests

The authors declare no competing interests.

Funding

This work was supported by the Agence Nationale de la Recherche (ANR-10-JCJC-1206, JCJC project ChromFlow to C.C.C.; ANR-22-CE20-0038, PRC project ChromSwitch to C.C.C. and J.K.), a CNRS-Higher Education Chair (position 0428-64 to C.C.C.), the University of Grenoble Alpes for an UGA-UJF Initiative Chair (to C.C.C.), a research fellowship of the French embassy in Germany (to J.E.), a Marie Curie Intra European Fellowship within the European Union's Seventh Framework Programme (FP7/2007–2013 (to J.E. and C.C.C.), the CEA Impulsion program and DRF PhD grant (to J-B.I, C.C.C and J.K.), and the Grenoble Alliance for Cell & Structural Biology (GRAL) and CBH-EUR-GS Graduate School (ANR-10-LABX-49-01 to J-B.I, C.C.C and J.K.; ANR-17-EURE-0003 to V.G.). Work in the Grasser lab was supported by the German research Foundation (DFG) through grant SFB960 to K.D.G. and work in the Probst/Tatout lab by the Agence Nationale de la Recherche grant SeedChrom (ANR-22-CE20-0028). MGX acknowledges financial support from France Génomique National infrastructure, funded as part of "Investissement d'Avenir" program managed by Agence Nationale pour la Recherche (contract ANR-10-INBS-09). The funders had no role in study design, data collection and analysis, decision to publish, or preparation of the manuscript.

Data availability

Epigenomics and transcriptomics data that support the findings of this study are available as article supplementary information material (Supplementary Tables). Corresponding raw data (ChIP-seq and RNA-seq on ULT1 series, as well as ChIP-seq on REF6 series) are openly available in the NCBI Sequence Read Archive repository platform (SRA) at http://www.ncbi.nlm.nih.gov/bioproject/1163278, (Bioproject reference number: PRJNA1163278). Microscopy images used for quantifications in Suppl. Fig. S5 are deposited on the OMERO server at https://omero.bio.fsu.edu/webclient/?show=project-5201.

775 **References**

776 **Antosz W, Pfab A, Ehrnsberger HF, Holzinger P, Köllen K, Mortensen SA, Bruckmann A, Schubert T, Längst**
777 **G, Griesenbeck J, *et al.* 2017**. The Composition of the Arabidopsis RNA Polymerase II Transcript Elongation
778 Complex Reveals the Interplay between Elongation and mRNA Processing Factors. *The Plant Cell* **29**: 854–
779 870.
780 **Aranda S, Mas G, Di Croce L**. **2015**. Regulation of gene transcription by Polycomb proteins. *Sci Adv* **1**:
781 e1500737.
782 **Berr A, Shafiq S, Shen WH**. **2011**. Histone modifications in transcriptional activation during plant
783 development. *Biochim Biophys Acta* **1809**: 567–76.
784 **Borg M, Jacob Y, Susaki D, LeBlanc C, Buendía D, Axelsson E, Kawashima T, Voigt P, Boavida L, Becker J,**
785 ***et al.* 2020**. Targeted reprogramming of H3K27me3 resets epigenetic memory in plant paternal chromatin.
786 *Nature Cell Biology* **22**: 621–629.
787 **Carles CC, Choffnes-Inada D, Reville K, Lertpiriyapong K, Fletcher JC**. **2005**. ULTRAPETALA1 encodes a SAND
788 domain putative transcriptional regulator that controls shoot and floral meristem activity in Arabidopsis.
789 *Development* **132**: 897–911.
790 **Carles CC, Fletcher JC**. **2009**. The SAND domain protein ULTRAPETALA1 acts as a trithorax group factor to
791 regulate cell fate in plants. *Genes & Development* **23**: 2723–8.
792 **Carles CC, Lertpiriyapong K, Reville K, Fletcher JC**. **2004**. The ULTRAPETALA1 gene functions early in
793 Arabidopsis development to restrict shoot apical meristem activity and acts through WUSCHEL to regulate
794 floral meristem determinacy. *Genetics* **167**: 1893–903.
795 **Chanvivattana Y, Bishopp A, Schubert D, Stock C, Moon Y-H, Sung ZR, Goodrich J**. **2004**. Interaction of
796 Polycomb-group proteins controlling flowering in Arabidopsis. *Development* **131**: 5263–5276.
797 **Czermin B, Melfi R, McCabe D, Seitz V, Imhof A, Pirrotta V**. **2002**. Drosophila enhancer of Zeste/ESC
798 complexes have a histone H3 methyltransferase activity that marks chromosomal Polycomb sites. *Cell* **111**:
799 185–96.
800 **Desset S, Poulet A, Tatout C**. **2018**. Quantitative 3D Analysis of Nuclear Morphology and Heterochromatin
801 Organization from Whole-Mount Plant Tissue Using NucleusJ. In: Bemer M, Baroux C, eds. Methods in
802 Molecular Biology. Plant Chromatin Dynamics. New York, NY: Springer New York, 615–632.
803 **Dubos T, Poulet A, Gonthier-Gueret C, Mougeot G, Vanrobays E, Li Y, Tutois S, Pery E, Chausse F, Probst**
804 **AV, *et al.* 2020**. Automated 3D bio-imaging analysis of nuclear organization by NucleusJ 2.0. *Nucleus* **11**:
805 315–329.
806 **Engelhorn J, Blanvillain R, Carles CC**. **2014**. Gene activation and cell fate control in plants: a chromatin
807 perspective. *Cell Mol Life Sci* **71**: 3119–37.
808 **Engelhorn J, Blanvillain R, Kröner C, Parrinello H, Rohmer M, Posé D, Ott F, Schmid M, Carles CC**. **2017a**.
809 Dynamics of H3K4me3 Chromatin Marks Prevails over H3K27me3 for Gene Regulation during Flower
810 Morphogenesis in Arabidopsis thaliana. *Epigenomes* **1**: 8.
811 **Engelhorn J, Wellmer F, Carles CC**. **2017b**. *Profiling histone modifications in synchronised floral tissues for*
812 *quantitative resolution of chromatin and transcriptome dynamics.* (Springer NY, Ed.). Methods Mol Biol.:
813 Methods Mol Biol.
814 **Fitzgerald DJ, Berger P, Schaffitzel C, Yamada K, Richmond TJ, Berger I**. **2006**. Protein complex expression
815 by using multigene baculoviral vectors. *Nature Methods* **3**: 1021–1032.
816 **Freese NH, Norris DC, Loraine AE**. **2016**. Integrated genome browser: visual analytics platform for
817 genomics. *Bioinformatics* **32**: 2089–2095.
818 **Ge SX, Jung D, Yao R**. **2020**. ShinyGO: a graphical gene-set enrichment tool for animals and plants (A
819 Valencia, Ed.). *Bioinformatics* **36**: 2628–2629.
820 **Godwin J, Farrona S**. **2022**. The Importance of Networking: Plant Polycomb Repressive Complex 2 and Its
821 Interactors. *Epigenomes* **6**: 8.

822 **Goodrich J, Puangsomlee P, Martin M, Long D, Meyerowitz EM, Coupland G**. **1997**. A Polycomb-group
823 gene regulates homeotic gene expression in Arabidopsis. *Nature* **386**: 44–51.
824 **Højfeldt JW, Hedehus L, Laugesen A, Tatar T, Wiehle L, Helin K**. **2019**. Non-core Subunits of the PRC2
825 Complex Are Collectively Required for Its Target-Site Specificity. *Molecular Cell* **76**: 423-436.e3.
826 **Huq E, Al-Sady B, Quail PH**. **2003**. Nuclear translocation of the photoreceptor phytochrome B is necessary
827 for its biological function in seedling photomorphogenesis. *The Plant Journal* **35**: 660–664.
828 **Jacob Y, Bergamin E, Donoghue MT, Mongeon V, LeBlanc C, Voigt P, Underwood CJ, Brunzelle JS, Michaels**
829 **SD, Reinberg D, *et al.* 2014**. Selective methylation of histone H3 variant H3.1 regulates heterochromatin
830 replication. *Science* **343**: 1249–53.
831 **Jiao L, Liu X**. **2015**. Structural basis of histone H3K27 trimethylation by an active polycomb repressive
832 complex 2. *Science* **350**: aac4383.
833 **Justin N, Zhang Y, Tarricone C, Martin SR, Chen S, Underwood E, De Marco V, Haire LF, Walker PA,**
834 **Reinberg D, *et al.* 2016**. Structural basis of oncogenic histone H3K27M inhibition of human polycomb
835 repressive complex 2. *Nature Communications* **7**: 11316.
836 **Kingston RE, Tamkun JW**. **2014a**. Transcriptional regulation by trithorax-group proteins. *Cold Spring Harbor*
837 *Perspectives in Biology* **6**: a019349.
838 **Kingston RE, Tamkun JW**. **2014b**. Transcriptional regulation by trithorax-group proteins. *Cold Spring Harb*
839 *Perspect Biol* **6**: a019349.
840 **Lee C-H, Holder M, Grau D, Saldana-Meyer R, Ganai RA, Zhang J, Wang M, Dobenecker M-W, Reinberg D,**
841 **Armache K-J**. **2018**. Distinct stimulatory mechanisms regulate the catalytic activity of Polycomb Repressive
842 Complex 2 (PRC2).
843 **Lee C-H, Yu J-R, Granat J, Saldaña-Meyer R, Andrade J, LeRoy G, Jin Y, Lund P, Stafford JM, Garcia BA, *et***
844 ***al.* 2019**. Automethylation of PRC2 promotes H3K27 methylation and is impaired in H3K27M pediatric
845 glioma. *Genes & Development* **33**: 1428–1440.
846 **Lopez-Vernaza M, Yang S, Muller R, Thorpe F, de Leau E, Goodrich J**. **2012**. Antagonistic roles of
847 SEPALLATA3, FT and FLC genes as targets of the polycomb group gene CURLY LEAF. *PLoS One* **7**: e30715.
848 **Lu F, Cui X, Zhang S, Jenuwein T, Cao X**. **2011**. Arabidopsis REF6 is a histone H3 lysine 27 demethylase. *Nat*
849 *Genet* **43**: 715–9.
850 **Margueron R, Li G, Sarma K, Blais A, Zavadil J, Woodcock CL, Dynlacht BD, Reinberg D**. **2008**. Ezh1 and
851 Ezh2 maintain repressive chromatin through different mechanisms. *Mol Cell* **32**: 503–18.
852 **Monfared MM, Carles CC, Rossignol P, Pires HR, Fletcher JC**. **2013**. The ULT1 and ULT2 trxG genes play
853 overlapping roles in Arabidopsis development and gene regulation. *Mol Plant* **6**: 1564–79.
854 **Moreau F, Thevenon E, Blanvillain R, Lopez-Vidriero I, Franco-Zorrilla JM, Dumas R, Parcy F, Morel P,**
855 **Trehin C, Carles CC**. **2016**. The Myb-domain protein ULTRAPETALA1 INTERACTING FACTOR 1 controls floral
856 meristem activities in Arabidopsis. *Development* **143**: 1108–19.
857 **Mougeot G, Safarbati S, Alégot H, Pouchin P, Field N, Almagro S, Pery É, Probst A, Tatout C, Evans DE, *et***
858 ***al.* 2024**. Biom3d, a modular framework to host and develop 3D segmentation methods.
859 **Mozgova I, Hennig L**. **2015**. The polycomb group protein regulatory network. *Annu Rev Plant Biol* **66**: 269–
860 96.
861 **Muller-Xing R, Clarenz O, Pokorny L, Goodrich J, Schubert D**. **2014**. Polycomb-Group Proteins and
862 FLOWERING LOCUS T Maintain Commitment to Flowering in Arabidopsis thaliana. *The Plant Cell* **26**: 2457–
863 2471.
864 **Pfab A, Antosz W, Holzinger P, Bruckmann A, Griesenbeck J, Grasser KD**. **2017**. Analysis of In Vivo
865 Chromatin and Protein Interactions of Arabidopsis Transcript Elongation Factors. In: Kaufmann K, Mueller-
866 Roeber B, eds. Methods in Molecular Biology. Plant Gene Regulatory Networks. New York, NY: Springer
867 New York, 105–122.
868 **Pfaffl MW, Horgan GW, Dempfle L**. **2002**. Relative expression software tool (REST©) for group-wise

869 comparison and statistical analysis of relative expression results in real-time PCR. *Nucleic Acids Research*
870 **30**.
871 **Pires HR, Monfared MM, Shemyakina EA, Fletcher JC**. **2014**. ULTRAPETALA trxG genes interact with
872 KANADI transcription factor genes to regulate Arabidopsis gynoecium patterning. *The Plant Cell* **26**: 4345–
873 61.
874 **Pu L, Liu MS, Kim SY, Chen LF, Fletcher JC, Sung ZR**. **2013**. EMBRYONIC FLOWER1 and ULTRAPETALA1 Act
875 Antagonistically on Arabidopsis Development and Stress Response. *Plant Physiol* **162**: 812–30.
876 **Ramírez F, Ryan DP, Grüning B, Bhardwaj V, Kilpert F, Richter AS, Heyne S, Dündar F, Manke T**. **2016**.
877 deepTools2: a next generation web server for deep-sequencing data analysis. *Nucleic Acids Research* **44**:
878 W160–W165.
879 **Sanulli S, Justin N, Teissandier A, Ancelin K, Portoso M, Caron M, Michaud A, Lombard B, da Rocha ST,**
880 **Offer J, *et al.* 2015**. Jarid2 Methylation via the PRC2 Complex Regulates H3K27me3 Deposition during Cell
881 Differentiation. *Mol Cell* **57**: 769–83.
882 **Schmitges FW, Prusty AB, Faty M, Stutzer A, Lingaraju GM, Aiwazian J, Sack R, Hess D, Li L, Zhou S, *et al.***
883 **2011**. Histone methylation by PRC2 is inhibited by active chromatin marks. *Mol Cell* **42**: 330–41.
884 **Schuettengruber B, Bourbon H-M, Di Croce L, Cavalli G**. **2017**. Genome Regulation by Polycomb and
885 Trithorax: 70 Years and Counting. *Cell* **171**: 34–57.
886 **Shu J, Chen C, Li C, Cui Y**. **2020**. The complexity of PRC2 catalysts CLF and SWN in plants. *Biochemical Society*
887 *Transactions* **48**: 2779–2789.
888 **Shu J, Chen C, Thapa RK, Bian S, Nguyen V, Yu K, Yuan Z-C, Liu J, Kohalmi SE, Li C, *et al.* 2019**. Genome-
889 wide occupancy of histone H3K27 methyltransferases CURLY LEAF and SWINGER in *Arabidopsis* seedlings.
890 *Plant Direct* **3**: e00100.
891 **Sun B, Looi L-S, Guo S, He Z, Gan E-S, Huang J, Xu Y, Wee W-Y, Ito T**. **2014**. Timing Mechanism Dependent
892 on Cell Division Is Invoked by Polycomb Eviction in Plant Stem Cells. *Science* **343**: 1248559–1248559.
893 **Trapnell C, Roberts A, Goff L, Pertea G, Kim D, Kelley DR, Pimentel H, Salzberg SL, Rinn JL, Pachter L**. **2012**.
894 Differential gene and transcript expression analysis of RNA-seq experiments with TopHat and Cufflinks. *Nat*
895 *Protoc* **7**: 562–78.
896 **Van Leene J, Eeckhout D, Cannoot B, De Winne N, Persiau G, Van De Slijke E, Vercruysse L, Dedecker M,**
897 **Verkest A, Vandepoele K, *et al.* 2015**. An improved toolbox to unravel the plant cellular machinery by
898 tandem affinity purification of Arabidopsis protein complexes. *Nature Protocols* **10**: 169–187.
899 **Wang X, Long Y, Paucek RD, Gooding AR, Lee T, Burdorf RM, Cech TR**. **2019**. Regulation of histone
900 methylation by automethylation of PRC2. *Genes & Development* **33**: 1416–1427.
901 **Wang D, Tyson MD, Jackson SS, Yadegari R**. **2006**. Partially redundant functions of two SET-domain
902 polycomb-group proteins in controlling initiation of seed development in *Arabidopsis*. *Proceedings of the*
903 *National Academy of Sciences* **103**: 13244–13249.
904 **Xu F, Kuo T, Rosli Y, Liu M-S, Wu L, Chen L-FO, Fletcher JC, Sung ZR, Pu L**. **2018**. Trithorax Group Proteins
905 Act Together with a Polycomb Group Protein to Maintain Chromatin Integrity for Epigenetic Silencing during
906 Seed Germination in Arabidopsis. *Molecular Plant* **11**: 659–677.
907 **Yan W, Chen D, Smaczniak C, Engelhorn J, Liu H, Yang W, Graf A, Carles CC, Zhou D-X, Kaufmann K**. **2018**.
908 Dynamic and spatial restriction of Polycomb activity by plant histone demethylases. *Nature Plants* **4**: 681–
909 689.
910 **Zang C, Schones DE, Zeng C, Cui K, Zhao K, Peng W**. **2009**. A clustering approach for identification of
911 enriched domains from histone modification ChIP-Seq data. *Bioinformatics* **25**: 1952–8.
912 **Zhou Y, Tergemina E, Cui H, Förderer A, Hartwig B, Velikkakam James G, Schneeberger K, Turck F**. **2017**.
913 Ctf4-related protein recruits LHP1-PRC2 to maintain H3K27me3 levels in dividing cells in *Arabidopsis*
914 *thaliana*. *Proceedings of the National Academy of Sciences* **114**: 4833–4838.

Figure 1

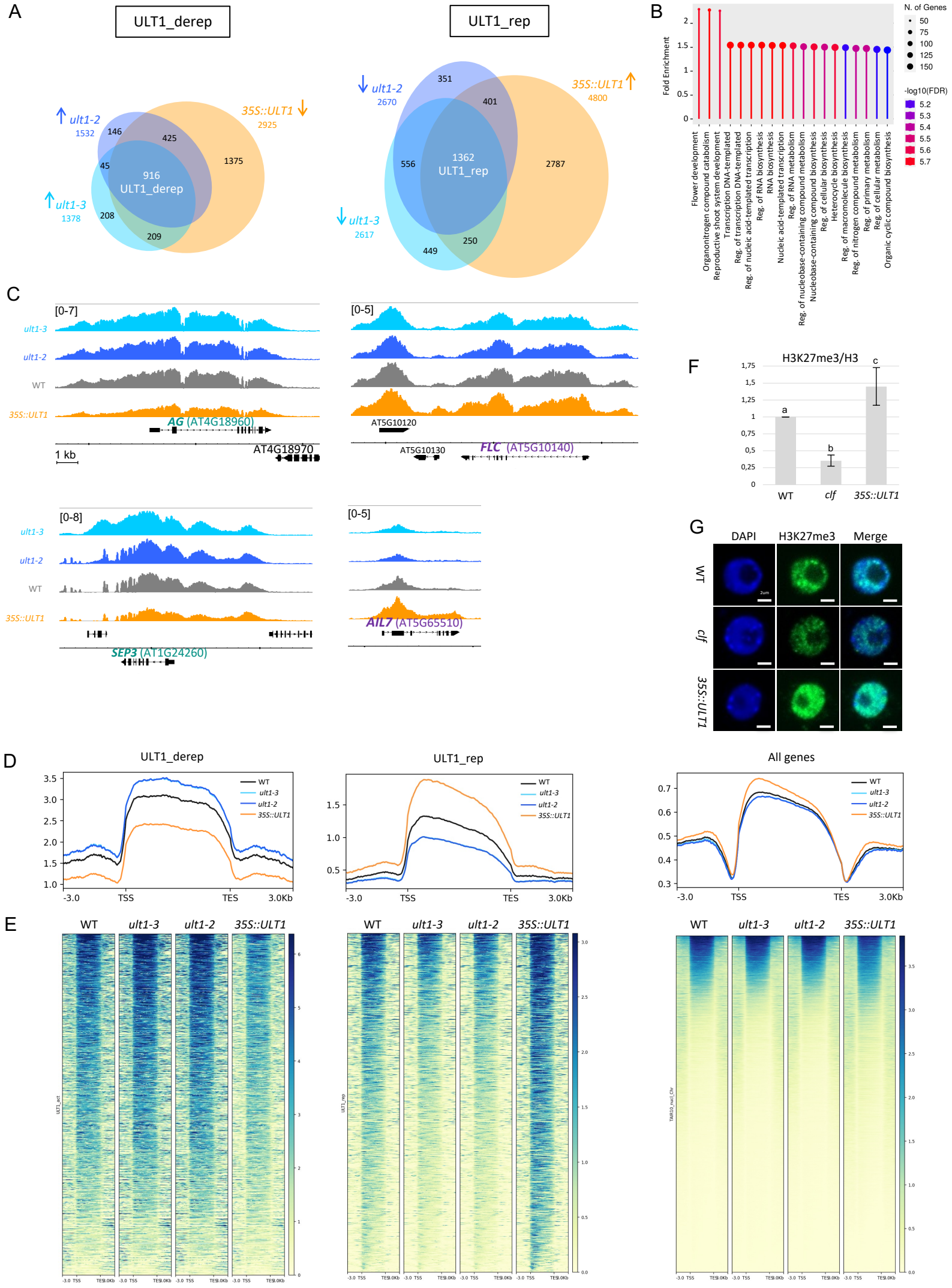
A
ULT1_derep
ULT1_rep
ult1-2
1532
35S::ULT1
2925
ult1-3
1378
146
425
1375
45
916
ULT1_derep
208
209
ult1-2
2670
351
401
35S::ULT1
4800
556
1362
ULT1_rep
2787
ult1-3
2617
449
250
B
Fold Enrichment
N. of Genes
50
75
100
125
150
-log10(FDR)
5.2
5.3
5.4
5.5
5.6
5.7
Flower development
Organonitrogen compound catabolism
Reproductive shoot system development
Transcription DNA-templated
Reg. of transcription DNA-templated
Reg. of nucleic acid-templated transcription
Reg. of RNA biosynthesis
RNA biosynthesis
Nucleic acid-templated transcription
Reg. of RNA metabolism
Reg. of nucleobase-containing compound metabolism
Nucleobase-containing compound biosynthesis
Reg. of cellular biosynthesis
Heterocycle biosynthesis
Reg. of macromolecule biosynthesis
Reg. of nitrogen compound metabolism
Reg. of primary metabolism
Reg. of cellular metabolism
Organic cyclic compound biosynthesis
C
[0-7]
ult1-3
ult1-2
WT
35S::ULT1
AG (AT4G18960)
1 kb
AT4G18970
[0-5]
AT5G10120
AT5G10130
FLC (AT5G10140)
[0-8]
SEP3 (AT1G24260)
[0-5]
AIL7 (AT5G65510)
F
H3K27me3/H3
a
b
c
WT
clf
35S::ULT1
G
DAPI
H3K27me3
Merge
WT
clf
35S::ULT1
D
ULT1_derep
ULT1_rep
All genes
WT
ult1-3
ult1-2
35S::ULT1
-3.0
TSS
TES
3.0Kb
E
WT
ult1-3
ult1-2
35S::ULT1

Figure 1. Global and genome-wide dual effect of ULT1 on H3K27me3 mark abundance.

(A-E) Genome-wide influence of ULT1 on H3K27me3 marks in 8 day-old seedlings (grown in long-day conditions at 18° C day / 16° C night) of ULT1 loss- and gain-of-function lines: WT (Ler wild type), *ult1-2* (EMS line, null mutant), *ult1-3* (T-DNA insertion line, null mutant) and *35S::ULT1* (ectopic over-expressor). **(F,G)** Global effect of ULT1 gain-of-function on H3K27me3 abundance in 8 day-old seedlings, assessed by western blot or *in cyto* immuno-fluorescence.

(A) Venn-diagram showing overlap between populations of genes (left) with significantly elevated H3K27me3 in *ult1* mutants and significantly reduced H3K27me3 in *35S::ULT1* (ULT_derep); and (right) with significantly reduced H3K27me3 in *ult1* mutants and significantly increased H3K27me3 in 35S::ULT1 (ULT1_rep). Numbers in the circles indicate the number of genes in the respective overlap, numbers under genotypes indicate the total number of significantly changed genes found in this genotype.

(B) Functional categorisation of ULT1_derep genes. ShinyGO v0.8 analysis for significantly over-represented Gene Ontology terms.

(C) Examples of influence of ULT1 on H3K27me3 marks. Genome browser (IGB) view of H3K27me3 determined by ChIP-seq in wild type, *ult1-2*, *ult1-3* and *35S::ULT1* lines at the (left) *AGAMOUS* (*AG*) and *SEPALLATA3* (*SEP3*) loci (examples of ULT_derep targets) and at the (right) *FLOWERING LOCUS C* (*FLC*) and *AINTEGUMENTA-LIKE 7* (*AIL7*) loci (examples of ULT_rep targets). Thick arrows indicate exons, thin lines represent introns. The min-max coverage values for each gene are given in brackets (same scale for all genotypes corresponding to each gene). Note that the oscillation of the data towards the 3'-end of the *SEP3* locus is caused by the mapping of (Ler) ecotype to the Columbia reference genome. *ult1-3* does not show this alteration since it was originally generated in Columbia and backcrossed.

(D) Metagenes for ULT1-derep, ULT1-rep genes, and all genes : profile of H3K27me3 in WT, *ult1-2*, *ult1-3* and *35S::ULT1* lines. Average distribution of H3K27me3 over ULT1-derep, ULT1-rep genes, and genome-wide. Genes are scaled to the same length (6kb), Panels represent data of one biological replicate, similar observations were made for the second replicate.

(E) Heatmaps for H3K27me3 distribution for all ULT1-derep, ULT1-rep genes, and genome-wide, ranked from (top line) the highest H3K27me3-marked to(bottom line) the lowest H3K27me3-marked gene in the WT.

(F) Quantification of H3K27me3 by western blot on 8 day-old seedlings. Mean was calculated from 3 replicates, for which H3K27me3 quantification was normalized to H3. Letters indicate significant differences between samples (Student's t-test, one sided paired, P-value < 0.05).

(G) Representative nuclei after immunofluorescence staining using an antibody directed against H3K27me3 in WT, *clf-2* and *35S::ULT1* seedlings. DNA was counterstained with DAPI.

Figure 2

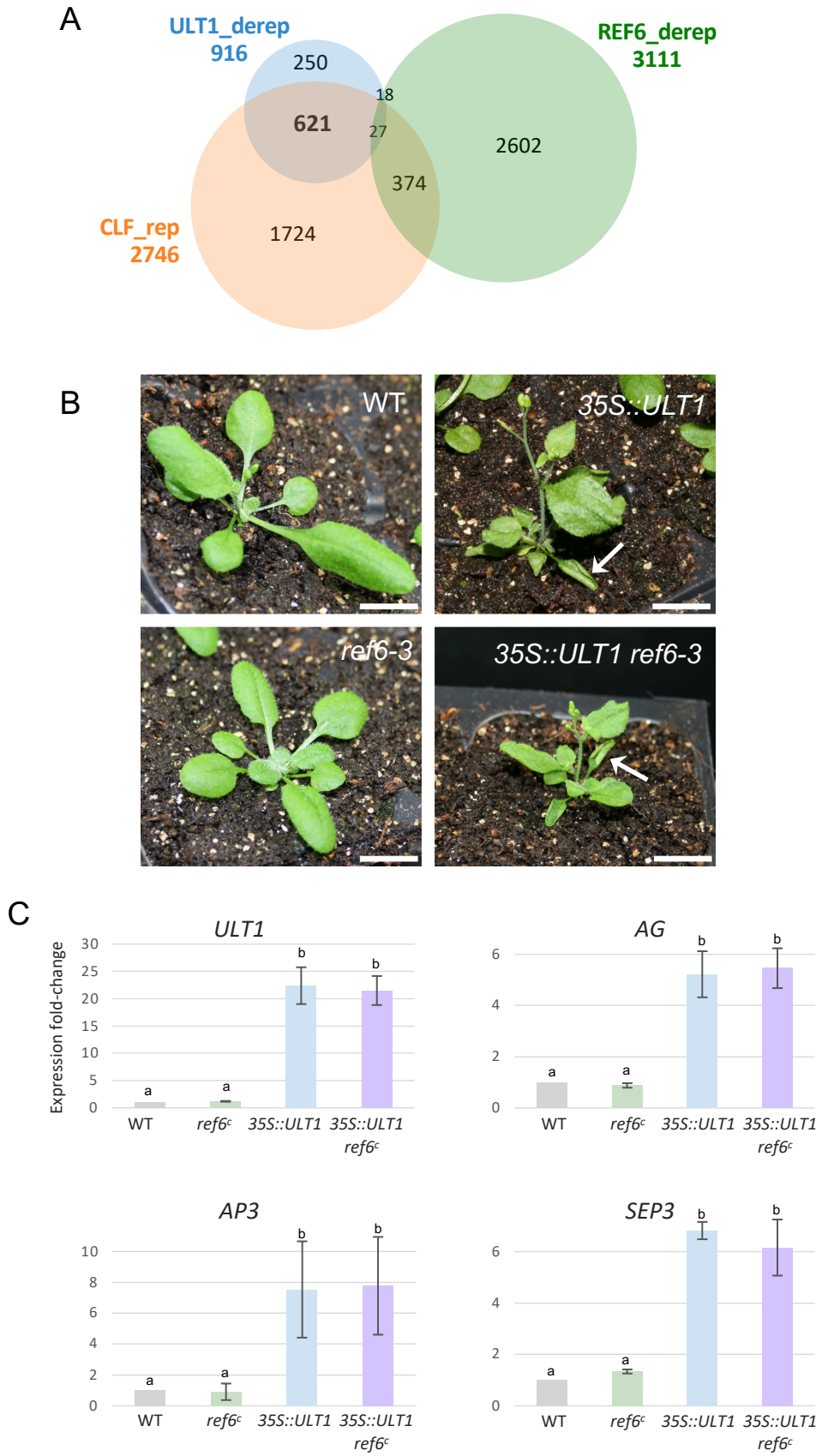

Figure 2. REF6 is dispensable for ectopic ULT1-induced phenotypes and de-repression of MADS floral genes.
(A) Venn-diagram showing overlap between populations of ULT1_derep genes with CLF_rep genes (genes with significantly reduced H3K27me3 in *clf*, re-analysis of raw data from Shu *et al*. 2019) and REF6_act genes (genes with significantly elevated H3K27me3 in *ref6*). **(B)** Pictures of 28 day-old Col-0 plants (WT, *35S::ULT1*, *ref6-3* mutant, *35S::ULT1 ref6-3), i*ndicating that 35S::ULT1 ectopic expression phenotypes do not depend on REF6 function. Arrows point at upward curling leaves in *35S::ULT1* and *35S::ULT1 ref6-3* plants. **(C)** Relative expression levels of *ULT1*, along with the homeotic floral genes *AG, AP3* and *SEP3* in 8-day-old seedlings (F3 *ref6C* x *35S::ULT1*), assessed by RT-qPCR. Expression levels of target genes were normalized with the reference gene *MON1*. Error bars correspond to standard deviation for 3 technical replicates. Letters indicate significant differences between samples (Student's t-test, one sided paired, P-value < 0.05). Similar results were obtained for 2 biological replicates.

Figure 3

A

AP-MS
(GS-ULT1)

A. thaliana cell culture

Protein	# peptides	Av. Mascot score
ULT1	42 - 45 - 45	3789
SWN	8 - 6 - 7	389
FIE	8 - 7 - 5	333
EOL1	20 - 33 - 10	478

B

C

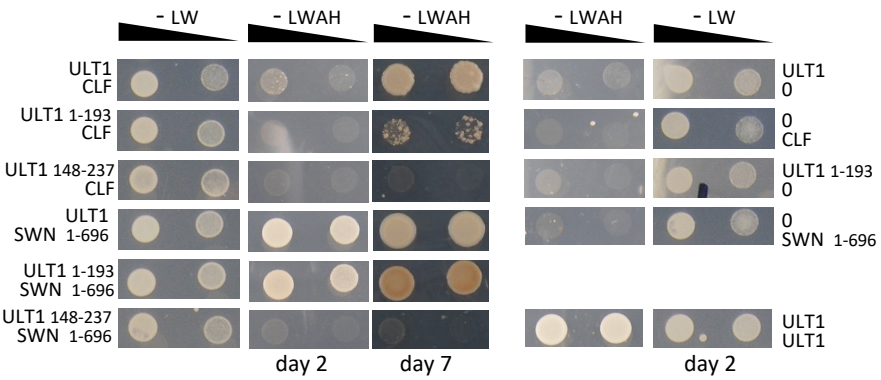

D

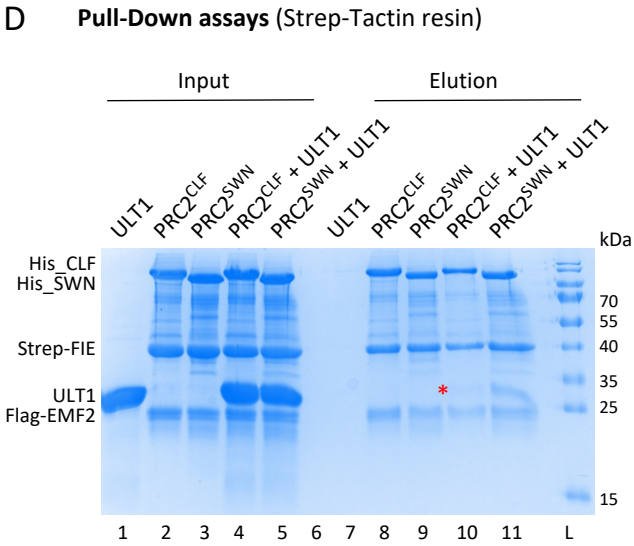

E

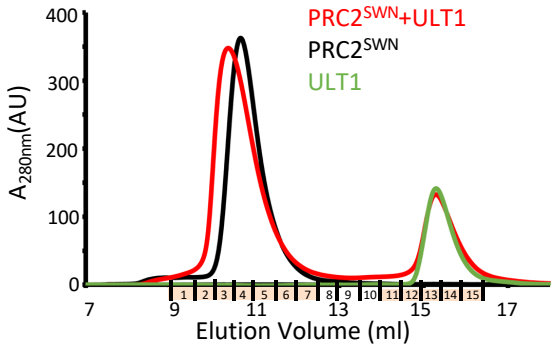

F

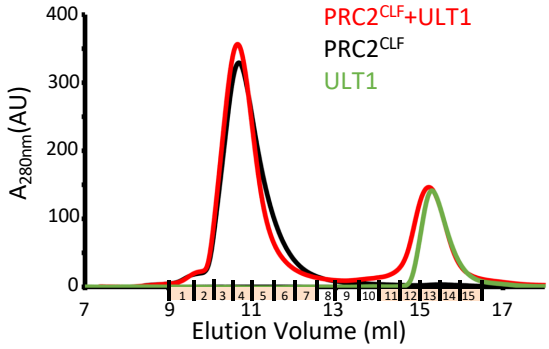

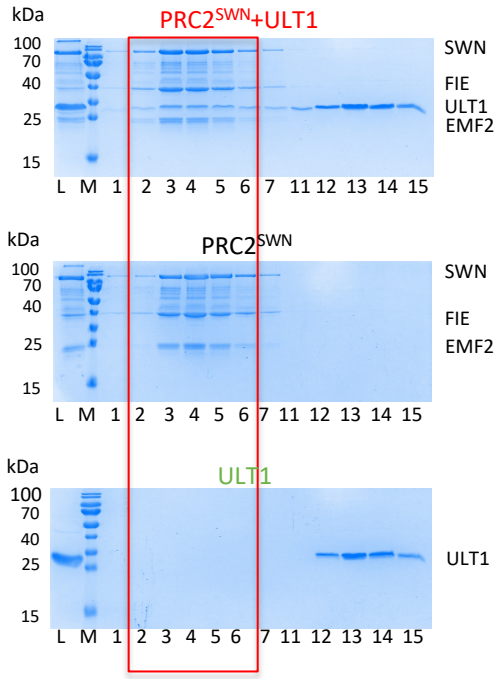

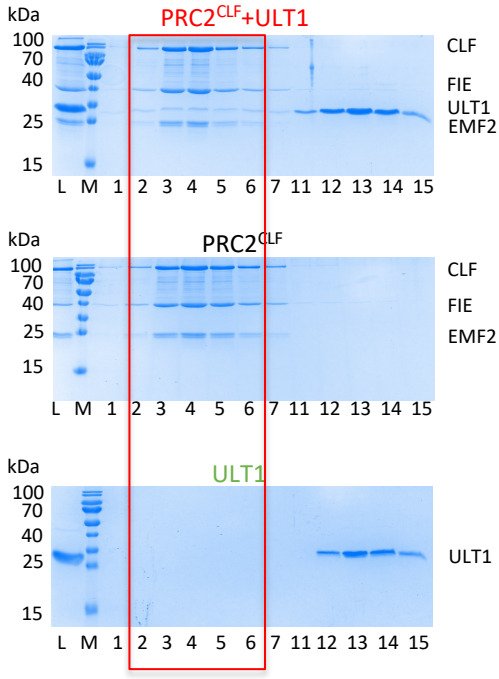

Figure 3. ULT1 physically interacts with PRC2 HMT CLF and SWN, *in vivo* and *in vitro*, with better affinity for SWN.

(A) AP-MS using GS-ULT1 in *Arabidopsis thaliana* cell cultures reveals components of the PRC2 complex. The numbers of unique peptides obtained for each replicate and the average mascot score out of 3 replicates are given.

(B) Schematic representation of ULT1 structure in domains.

(C) Yeast-two-hybrid assays for interaction tests between ULT1 (full-length, $ULT1_{1-193}$ and $ULT1_{148-237}$) and CLF or SWN. Photographs were taken after 2 days or 7 days of yeast growth, at two concentrations corresponding to optical densities at 600 nm (OD) of 10 and 1. The ULT1-ULT1 interaction was used as positive control.

(D) Strep-tag pull-down experiments of $PRC2^{SWN}$ and $PRC2^{CLF}$ complexes with untagged ULT1. Catalytic lobes of $PRC2^{SWN}$ and $PRC2^{CLF}$ contained a Strep-tag on the FIE subunit. All proteins were first purified by affinity chromatography and gel filtration. Proteins were mixed as indicated above the lanes. Input (lanes 1–5) and the eluates (lanes 7–11) were analyzed on 15% SDS-PAGE gels stained with Coomassie brilliant blue. The red asterisk indicates position of ULT1 in the elutions. $PRC2^{SWN}$ copurifies more efficiently with ULT1 than $PRC2^{CLF}$ (compare lanes 10 and 11).

(E) Overlay of Superdex 200 gel filtration elution profiles of the catalytic lobe of $PRC2^{SWN}$, ULT1 and their mixture. Lower panels show SDS-PAGE analysis of fractions 1-7 and 11-15 corresponding to the two major elution peaks. The red rectangle highlights fraction where ULT1 co-elutes with $PRC2^{SWN}$.

(F) Overlay of Superdex 200 gel filtration elution profiles of the catalytic lobe of $PRC2^{CLF}$, ULT1 and their mixture. Lower panels show SDS-PAGE analysis of fractions 1-7 and 11-15 corresponding to the two major elution peaks. The red rectangle highlights fraction where ULT1 co-elutes with $PRC2^{CLF}$. ULT1 is, however, sub-stoichiometric and there is essentially no shift of the elution peak compared to $PRC2^{CLF}$alone. The elution profile and corresponding SDS-PAGE gel of ULT1 is the same in panel E and F.

Figure 4

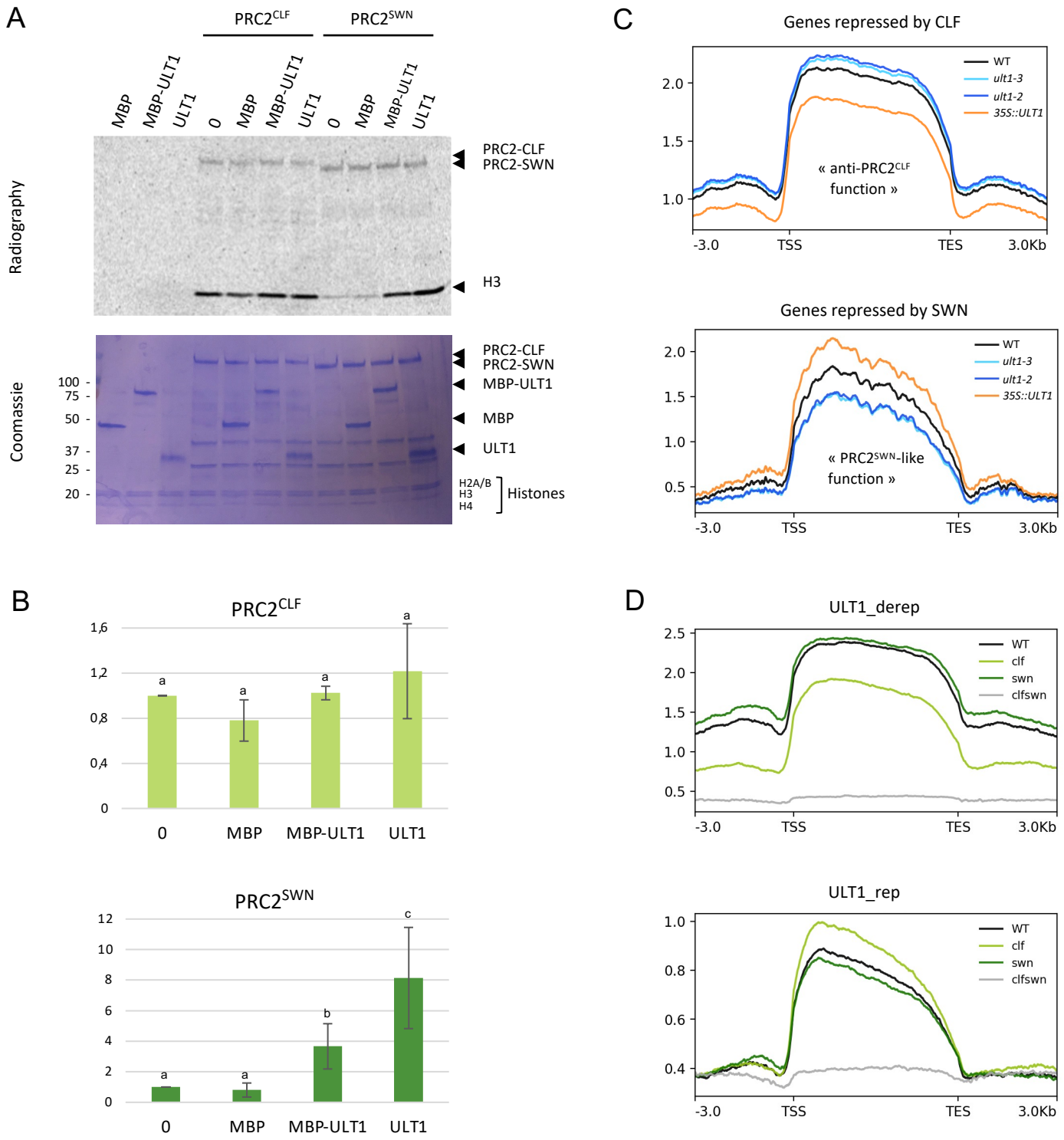

Figure 4. ULT1 increases PRC2-SWN HMT activity and displays a genome-wide PRC2^{SWN}-like function versus an anti-PRC2^{CLF}function.

(A-B) *in vitro* HMT activity tests on recombinant nucleosomes indicate that ULT1 significantly increases PRC2^{SWN} activity but not PRC2^{CLF} activity. (A) Top panel shows autoradiography of a SDS-PAGE gel after incubation of PRC2^{CLF} or PRC2^{SWN} (1.5ug of complex) without or with MBP, MBP-ULT1 or ULT1. Bottom panel shows Coomassie staining of the same SDS-PAGE. (B) Graphs showing relative quantifications of HMT activities in absence (0, MBP) or presence of ULT1 (MBP-ULT1, ULT1), for PRC2^{CLF} and PRC2^{SWN}. Error bars correspond to standard deviation for 3 replicates. Letters indicate significant differences between samples (Student's t-test, one sided paired, P-value < 0.05).

(C-D) Metagenes reveal an anti-PRC2^{CLF} function and a PRC2^{SWN}-like function for ULT1. (C) Mean H3K27me3 levels on genes targeted for repression by CLF (upper panel) or by SWN (lower panel), as observed in WT, *ult1-2, ult1-3* and *35S::ULT1* lines. (D) Mean H3K27me3 levels on genes de-repressed (upper panel) or repressed (lower panel) by ULT1, as observed in WT, *clf-2, swn* and *clf swn* mutants.

Figure 5

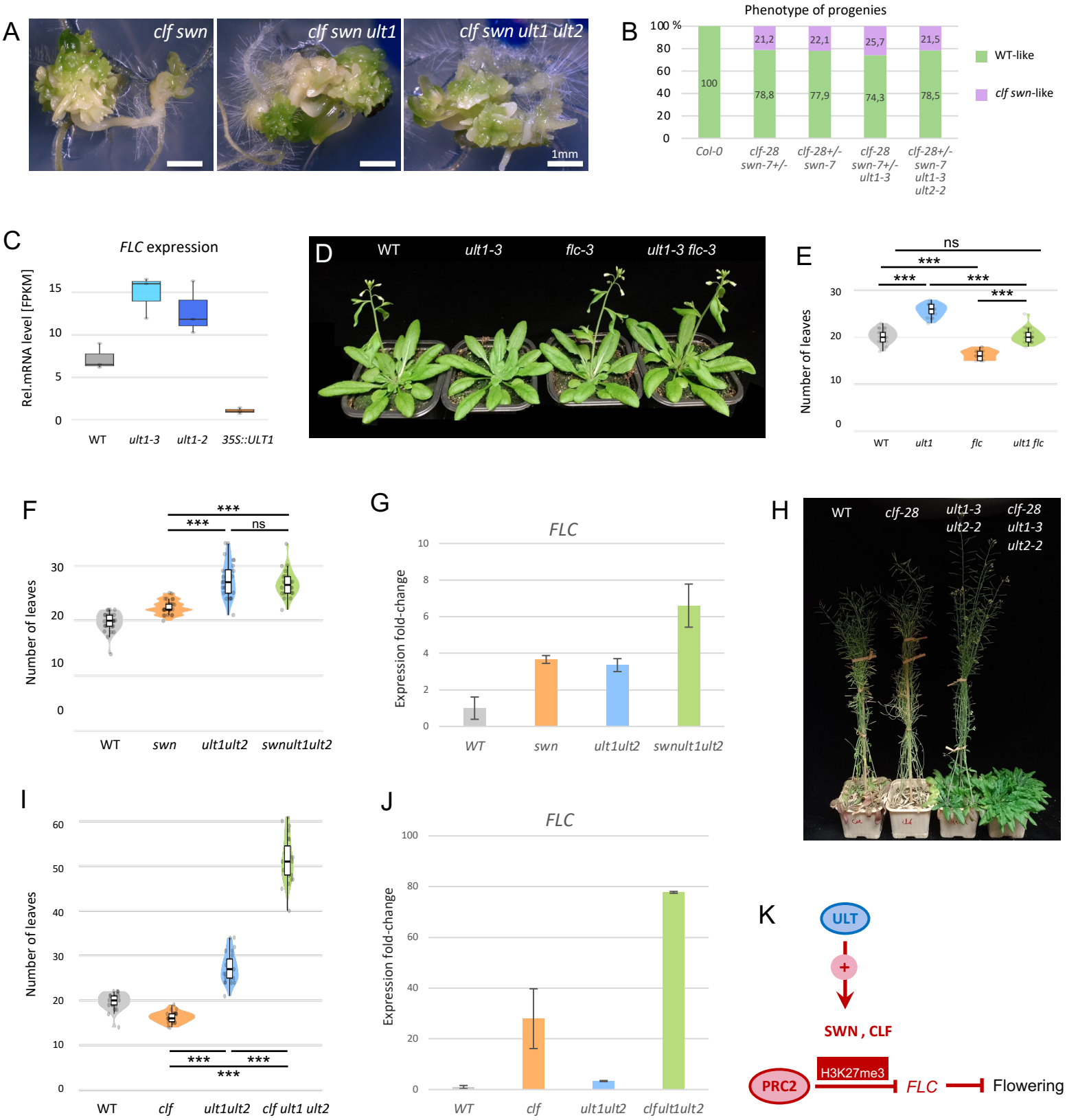
A
clf swn
clf swn ult1
clf swn ult1 ult2
1mm
B
Phenotype of progenies
100 %
80
60
40
20
0
100
21,2
78,8
22,1
77,9
25,7
74,3
21,5
78,5
Col-0
clf-28 swn-7+/-
clf-28+/- swn-7
clf-28 swn-7+/- ult1-3
clf-28+/- swn-7 ult1-3 ult2-2
WT-like
clf swn-like
C
FLC expression
Rel.mRNA level [FPKM]
15
10
5
0
WT
ult1-3
ult1-2
35S::ULT1
D
WT
ult1-3
flc-3
ult1-3 flc-3
E
ns
***
***
***
***
Number of leaves
30
20
10
0
WT
ult1
flc
ult1 flc
F
***
***
ns
Number of leaves
30
20
10
0
WT
swn
ult1ult2
swnult1ult2
G
FLC
Expression fold-change
10
8
6
4
2
0
WT
swn
ult1ult2
swnult1ult2
H
WT
clf-28
ult1-3 ult2-2
clf-28 ult1-3 ult2-2
I
Number of leaves
60
50
40
30
20
10
0
***
***
***
WT
clf
ult1ult2
clf ult1 ult2
J
FLC
Expression fold-change
100
80
60
40
20
0
WT
clf
ult1ult2
clfult1ult2
K
ULT
+
SWN , CLF
PRC2
H3K27me3
FLC
Flowering

Figure 5. ULT functions in a common pathway with PRC2 for flowering time and FLC regulation.

(A,B) *ult* loss-of-function does not complement sporophytic *prc2* mutant phenotypes. Pictures of double *clf-28 swn-7, triple clf-28 swn-7 ult1-3* and quadruple *clf-28 swn-7 ult1-3 ult2-2* mutants grown for 1 month. All genotypes grow as callus-like tissue with random organs arising in a dis-organized phyllotaxy: ectopic roots, somatic embryos, shoot-like structures. Scale bar: 1mm. Phenotyes of progenies of double *clf-28/+ swn-7, triple clf-28/+ swn-7 ult1-3* and quadruple *clf-28/+ swn-7 ult1-3 ult2-2* mutants, scored 10 days after sowing. Distribution of populations are given in percentages, calculated from 200 plants per progeny.

(C) Relative transcript levels (FPKM) on *FLC* from RNA-seq data from *ult1-3, ult1-2* mutants and 35S::ULT1 in 8-day-old seedlings grown under LD conditions at 18° C.

(D-E) Introduction of *flc-3* mutation rescues the late-flowering phenotype of *ult1*. (D) Representative Col-0, *ult1-3*, *flc-3* and *ult1-3 flc-3* mutant strains. (E) Flowering time of Col-0 and *ult1-3*, *flc-3* and *ult1-3 flc-3* mutant strains measured as rosette leaves at bolting.

(F-G) ULT1 functions in the same pathway as SWN for *FLC* regulation. (F) Flowering time of Col-0, *swn-7, ult1-3 ult2-2* and *swn-7 ult1-3 ult2-2* mutant strains measured as rosette leaves at bolting. (G) Transcript levels of *FLC* measured by qRT-PCR in Col-0, *swn-7, ult1-3 ult2-2* and *swn-7 ult1-3 ult2-2* in 8-day-old seedlings grown under LD conditions at 18° C.

(H-J) ULT1 functions in the same pathway as CLF for *FLC* regulation. (H) Representative Col-0, *clf-28, ult1-3 ult2-2* and *clf-28 ult1-3 ult2-2* mutant plants grown at LD 20 ° C. (I) Flowering time of Col-0, *clf-28, ult1-3 ult2-2* and *clf-28 ult1-3 ult2-2* measured as rosette leaves at bolting. (J) Transcript levels of *FLC* measured by qRT-PCR in Col-0, *clf-28, ult1-3 ult2-2* and *clf-28 ult1-3 ult2-2* in 8-day-old seedlings grown under LD conditions at 18° C. *FLC* expression is strongly upregulated in the triple *clf-28 ult1-3 ult2-2* mutant as compared to the double *ult1-3 ult2-2* mutant (Student's t-test, one sided paired, P-value< 0.05).

In E, F, I, symbols for significant differences correspond to: * P-value < 0.05, ** P-value < 0.01, *** P-value < 0.001; ns: no significant difference (for P-value <0.05).

(K) Model for *FLC* regulation by ULT1 and PRC2. ULT1 functions together with SWN to promote *FLC* repression, in a pathway synergistic to CLF.

Suppl. Table S1. Lists of ULT1_derep and ULT1_rep target genes.

Four sheets are displayed in the file, which correspond to, in order: all 916 ULT1_derep genes; subset of ULT1_derep genes that encode meristem, flowering and flower morphogenesis regulators; all 1362 ULT1_rep genes; subset of ULT1_rep genes that encode meristem, flowering and flower morphogenesis regulators.

→ *See excel File*

Suppl. Figure S1

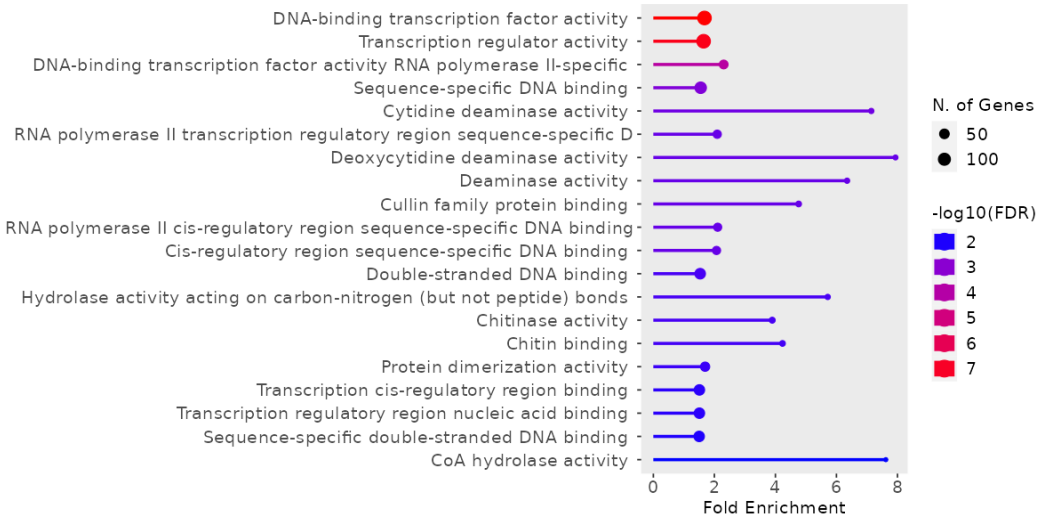

Suppl. Figure S1. Functional categorisaiton of ULT1_derep and ULT1_rep genes.
ShinyGO v0.8 analysis for significantly over-represented Gene Ontology terms among ULT1_derep genes compared to H3K27me3 target genes in Ler WT.

Suppl. Figure S2

A ULT1_derep genes: H3K27me3 mark profile

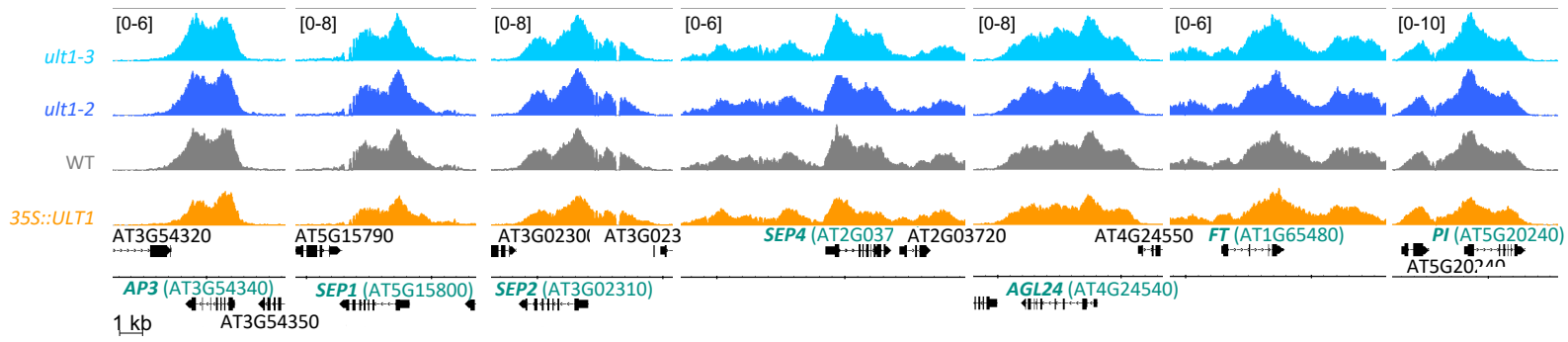

B ULT1_derep genes: H3K4me3 mark profile

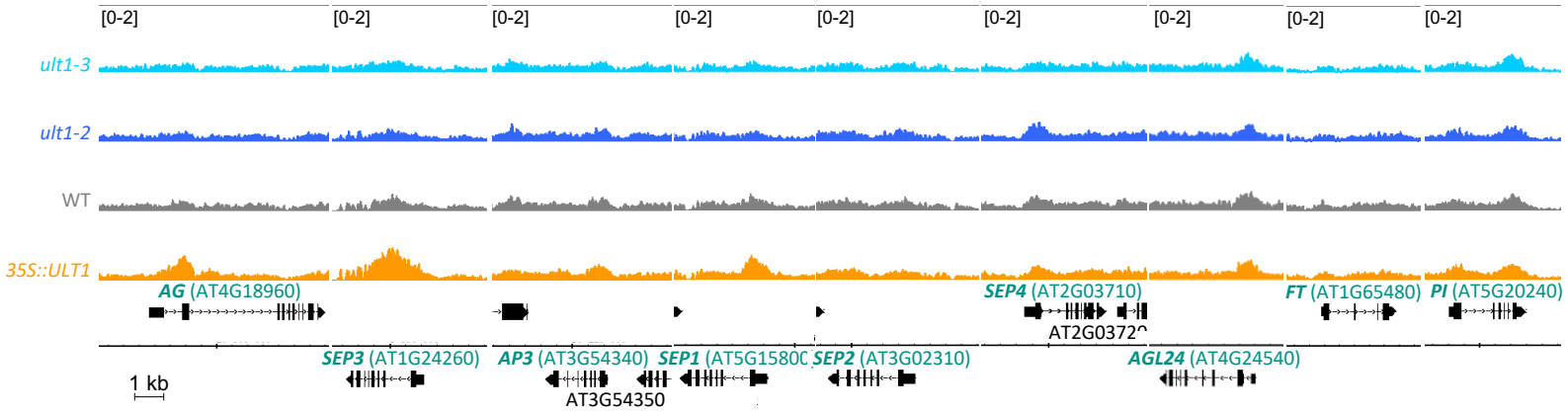

C ULT1_rep genes: H3K27me3 mark profile

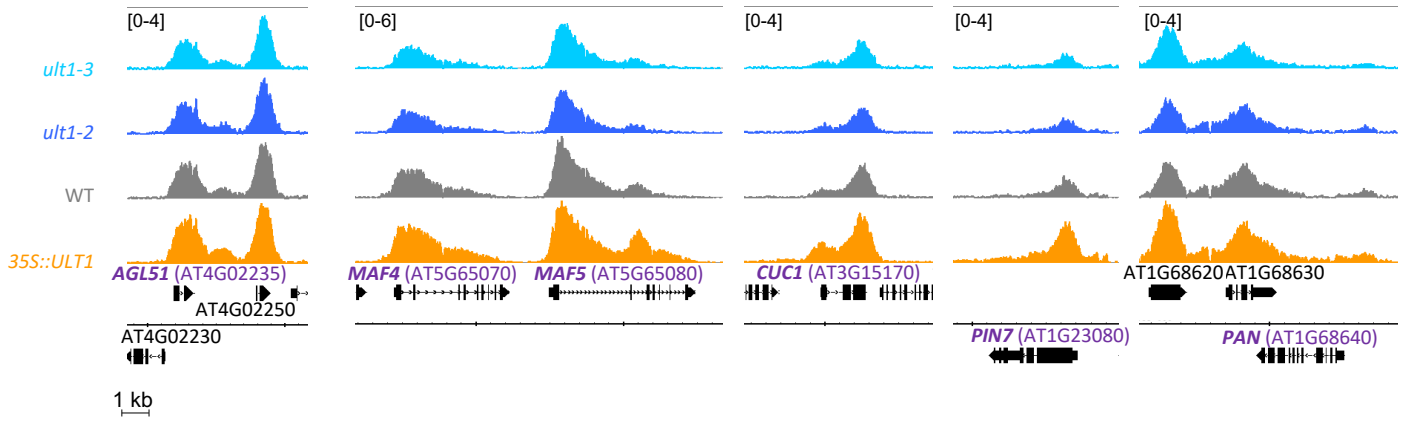

D ULT1_rep genes: H3K4me3 mark profile

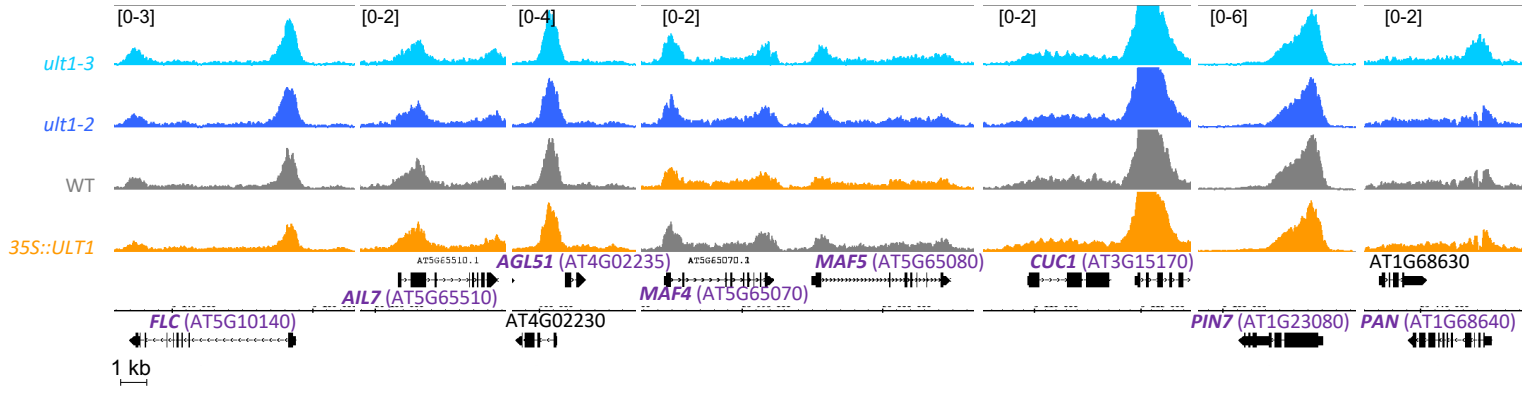

Suppl. Figure S2. Examples of influence of ULT1 on histone marks.

Genome browser (IGB) views of (A,C) H3K27me3 and (B,D) H3K4me3 mark profiles, as determined by ChIP-seq in wild type (Ler), *ult1-2* (EMS line, null mutant), *ult1-3* (T-DNA insertion line, null mutant) and *35S::ULT1*. Data is shown for (A-B) the ULT1_derep flower morphogenesis genes *APETALA3* (*AP3*), *SEPALLATA 1-4* (*SEP1,2,4*), *AP1, PISTILLATA* (*PI*) and the flowering regulators *AGAMOUS-LIKE 24* (*AGL24*) and *FLOWERING LOCUS T* (*FT*), and for the ULT1_rep genes *AGAMOUS-LIKE LOCUS 51* (*AGL51*), *FLOWERING LOCUS C* (*FLC*), master regulator of the reproductive transition and its paralogues MADS AFFECTING FLOWERING 4 (MAF4) and MAF5, the meristem regulators *AINTEGUMENTA-LIKE 7* (*AIL7*), CUP-SHAPED COTYLEDON1 (CUC1), ARABIDOPSIS PIN-FORMED 7 (PIN7) and PERIANTHIA (PAN); unless already shown in Figure 1 for H3K27me3.

Suppl. Figure S3

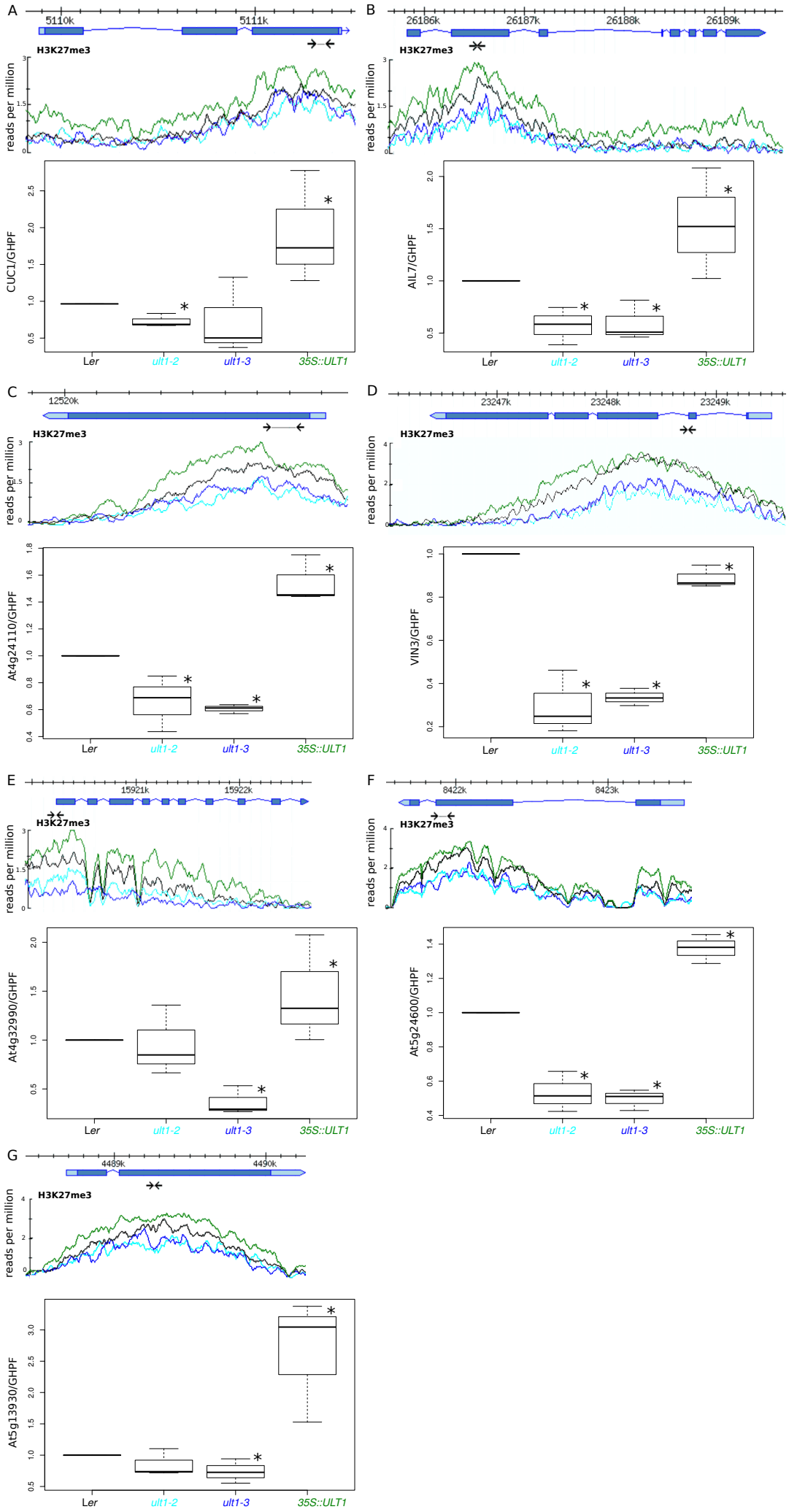

Suppl. Figure S3. ChIP q-PCR analysis of H3K27me3 abundance in *ult1-2, ult1-3* and *35S::UL*T1 at seven selected ULT1_rep genes.

AT3G62710 (Glycosyl hydrolase family protein - GHFP) was used to normalise the ChIP signal. Box plots show combined data of three biological replicates, the horizontal line displays the median, the whiskers mark the upper and lower values, the box represents the 25 % above and below the median. * reflects to statistical significance with Kruskal-Wallis test followed by post-hoc non-parametric two-sided Tuckey test, using the R package nparcomp (Knell, 2013). For comparison, the ChIP-seq results over each locus are included and the employed primers are indicated by arrows below the gene model. A: *CUC1*, B: *AIL7*, C: At4g24110, D: *VIN3*, E: At4g32990, F: At5g24600, G: At5g13930.

Suppl. Figure S4

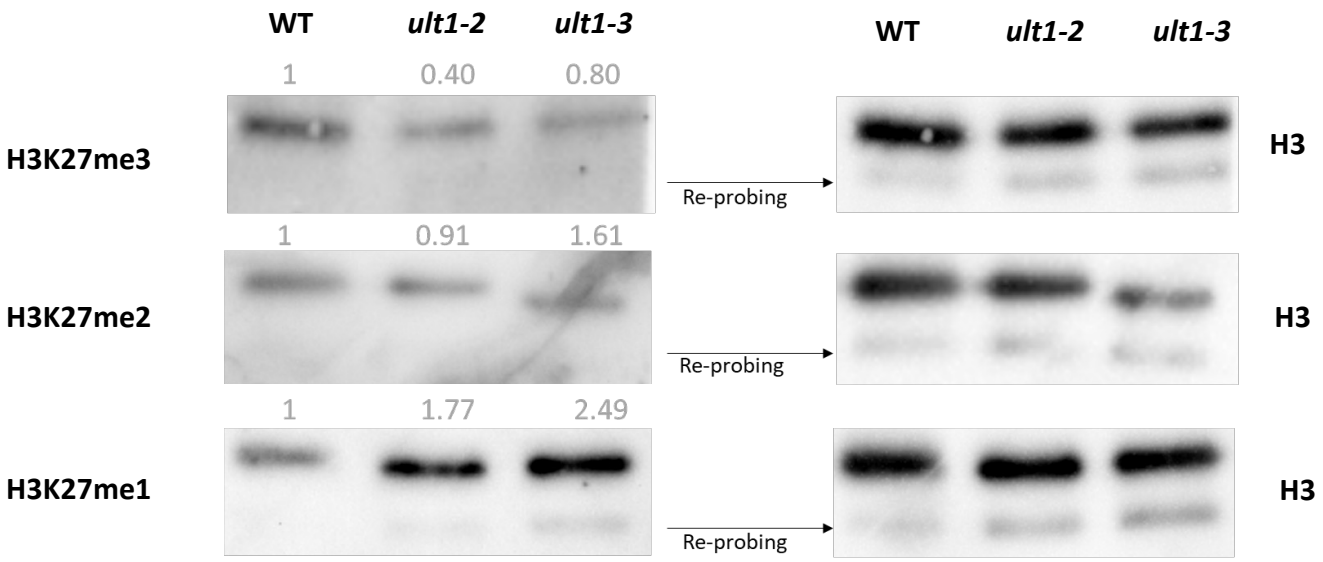

Suppl. Figure S4. Western blots for H3K27me1, me2, me3 in *ult1* lof mutant lines.
The same membrane was reprobed with the H3 antibody.

Suppl. Figure S5

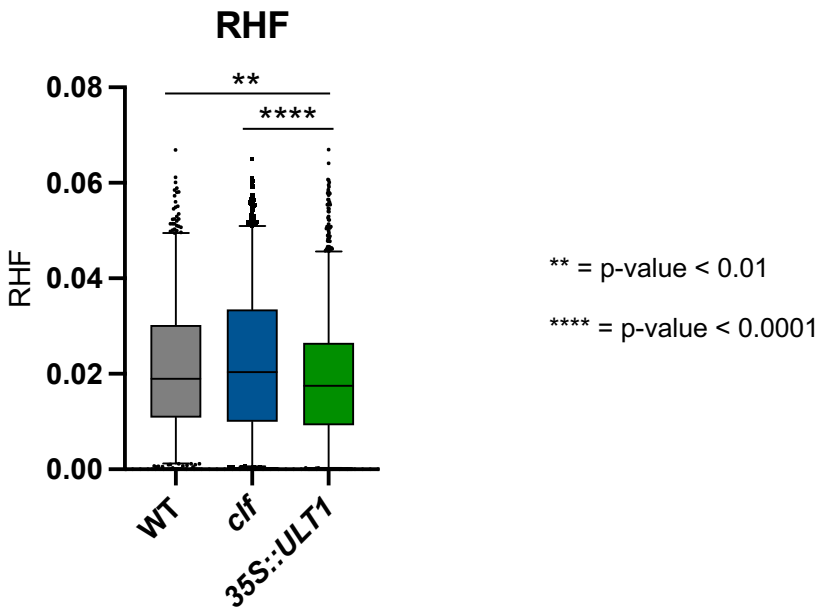

Suppl. Figure S5. Relative heterochromatin fraction (RHF=total volume of chromocenter spots / Volume of nucleus), quantified after Hoechst staining. Boxplots show the RHF determined in cotyledon epidermis nuclei from 14-days old WT (n=607), *clf-2* mutant (n=1072) and *35S::ULT1* (n=1262) seedlings. Statistical significant differences were determined by an ordinary one way Anova followed by Tukey's multiple comparisons test. The *clf* mutant shows a slight RHF increase compared to WT, while the *35S::ULT1* line displays a RHF decrease relative to WT and to *clf*. These effects were observed in a reproducible manner, in two independent experiments.

Suppl. Table S2. RNA-seq data with the full list of *Arabidopsis thaliana* genes and log2FC between ULT1 lof or ULT1 gof and control WT Ler. Three sheets are displayed for differences between *ult1-3,* or ult1-2 or 35S::ULT1 and Ler WT.

→ *See excel File*

Suppl. Table S3. Lists of genes up and down regulated in the different ULT1lof and ULT1gof lines.

Five sheets are displayed in the file, which correspond to, in order: targets targets down-regulated in *ult1-3*, down-regulated in *ult1-2*, down-regulated in *35S::ULT1,* up-regulated in *ult1-3*, up-regulated in *ult1-2*, up-regulated in *35S::ULT1*. P-values were calculated by hypergeometric testing.

→ *See excel File*

Suppl. Figure S6

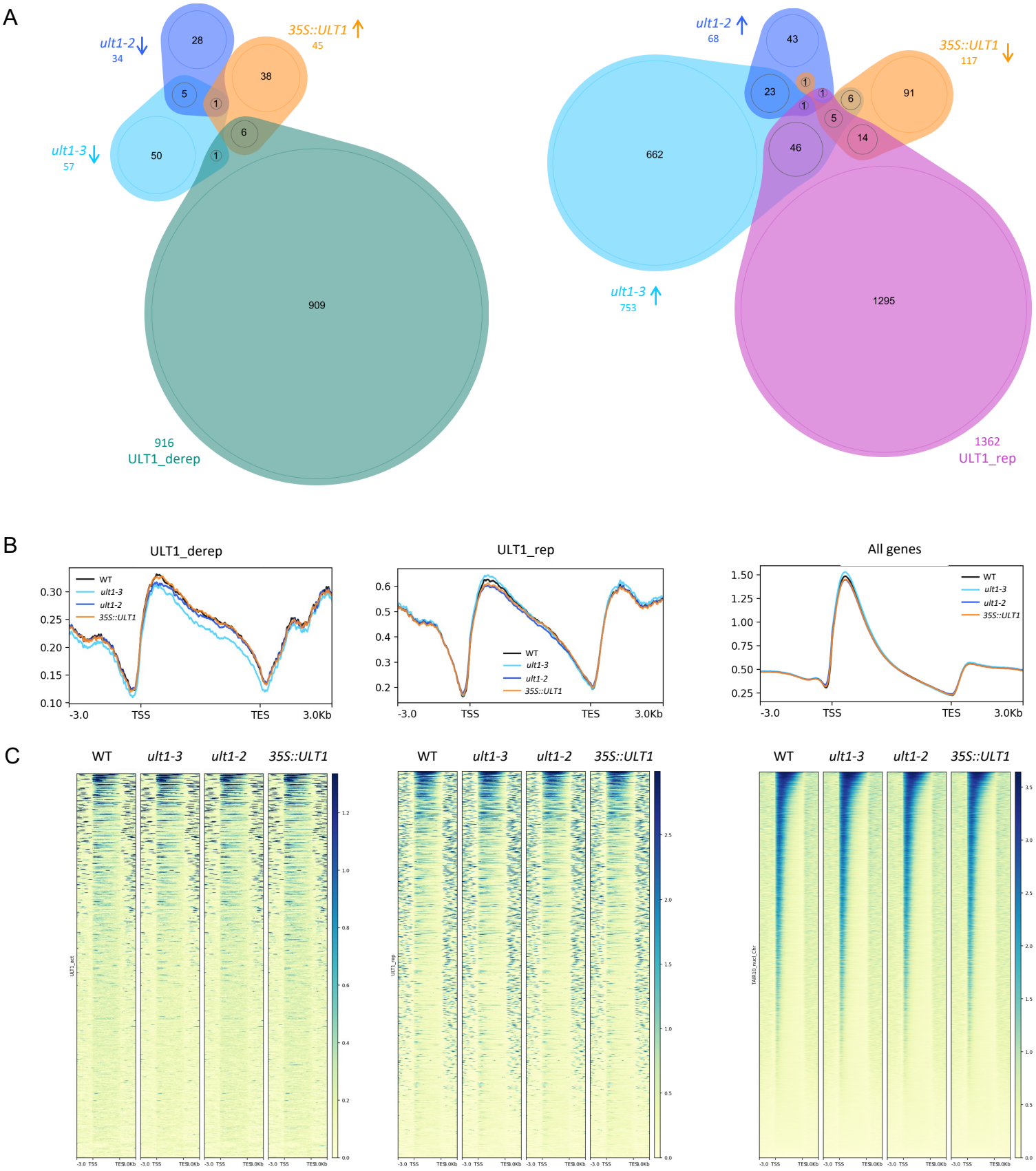

Suppl. Figure S6. Genome-wide influence of ULT1 on H3K4me3 marks in 8 day-old seedlings (grown in long-day conditions at 18° C day / 16° C night) **of ULT1 loss- and gain-of-function lines**: WT (Ler wild type), *ult1-2* (EMS line, null mutant), *ult1-3* (T-DNA insertion line, null mutant) and 35S::ULT1 (ectopic surexpressor).

(A) Venn-diagram showing overlaps between populations of genes (left) with significantly reduced H3K4me3 in *ult1-2* and *ult11-3*, significantly elevated H3K4me3 in 35S::ULT1 and H3K27me3 ULT1_derep genes; and (right) with significantly elevated H3K4me3 in *ult1-2* and *ult1-3*, significantly decreased H3K4me3 in 35S::ULT1 and H3K27me3 ULT1_rep genes. Numbers in the ellipses indicate the number of genes in the respective overlap, numbers under genotypes/gene sets indicate the total number of significantly changed genes found in this genotype/gene set. **(B)** Metagenes for ULT1-derep and ULT1-rep genes: profile of H3K4me3 in WT, *ult1-2*, *ult1-3* and *35S::ULT1* lines. Average distribution of H3K27me3 over ULT1-derep and ULT1-rep genes, and genome-wide. Genes are scaled to the same length (6kb). **(C)** Heatmaps for H3K4me3 distribution for all ULT1-derep and ULT1-rep genes, and genome-wide, ranked from (top line) the highest H3K4me3-marked to(bottom line) the lowest H3K4me3-marked gene in the WT.

Suppl. Figure S7

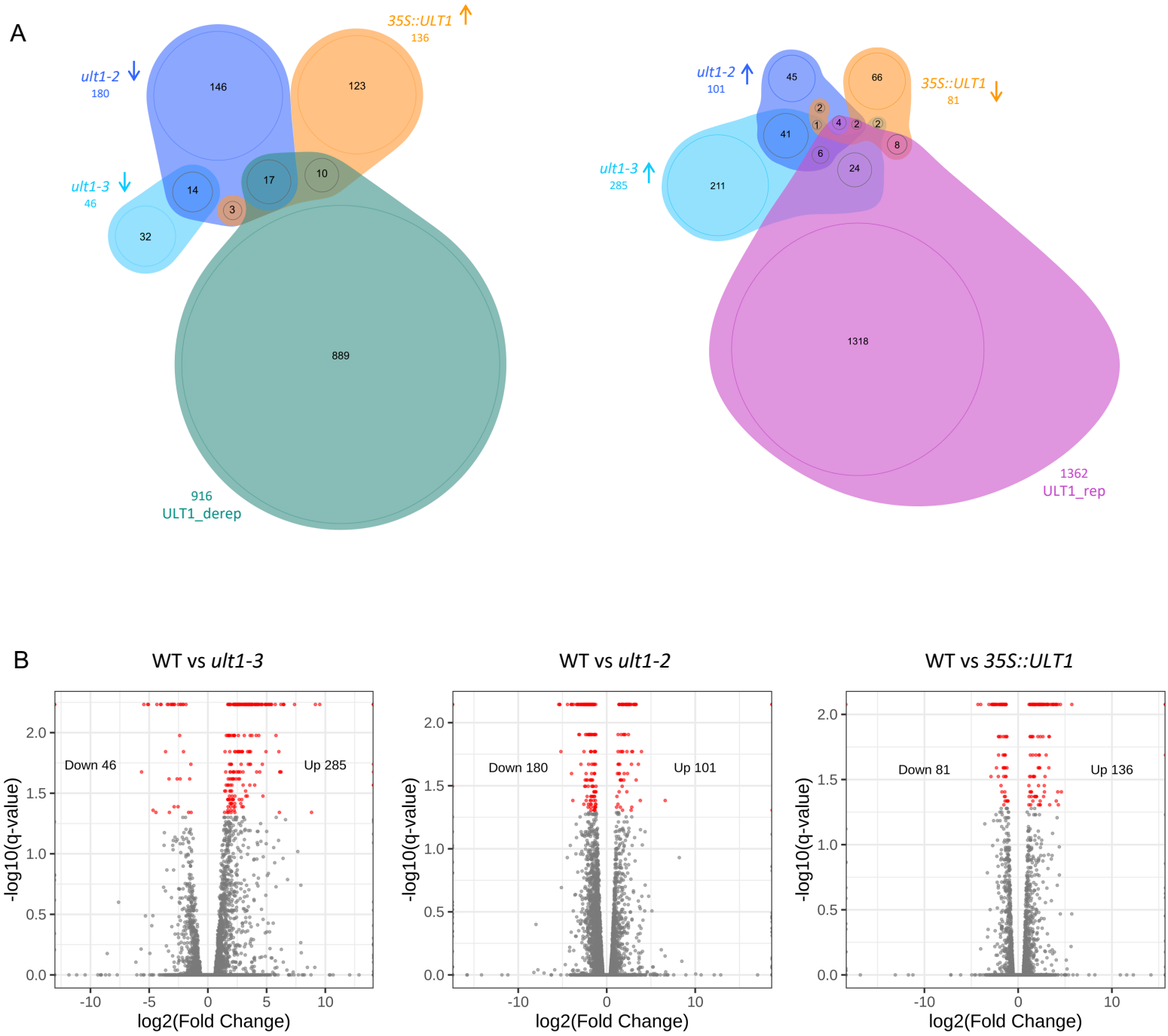

Suppl. Figure S7. Genome-wide influence of ULT1 on gene expression in 8 day-old seedlings (grown in long-day conditions at 18° C day / 16° C night) **of ULT1 loss- and gain-of-function lines**: WT (Ler wild type), *ult1-2* (EMS line, null mutant), *ult1-3* (T-DNA insertion line, null mutant) and 35S::ULT1 (ectopic surexpressor).

(A) Venn-diagram showing overlaps between populations of genes (left) with significantly reduced expression in *ult1-2* and *ult11-3*, significantly elevated expression *in 35S::ULT1* and H3K27me3 ULT1_derep genes; and (right) with significantly elevated expression in *ult1-2* and *ult1-3*, signficantly decreased expression in *35S::ULT1* and H3K27me3 ULT1_rep genes. Numbers in the ellipses indicate the number of genes in the respective overlap, numbers under genotypes/gene sets indicate the total number of signi cantly changed genes found in this genotype/gene set.

(B) Volcano plots showing log2(Fold Change) and –log10(q-value) for all Arabidopsis genes in each genotype comparison. Red dots represent genes showing significant changes in expression between two genotypes, grey dots are genes showing no significant differential expression.

Suppl. Figure S8

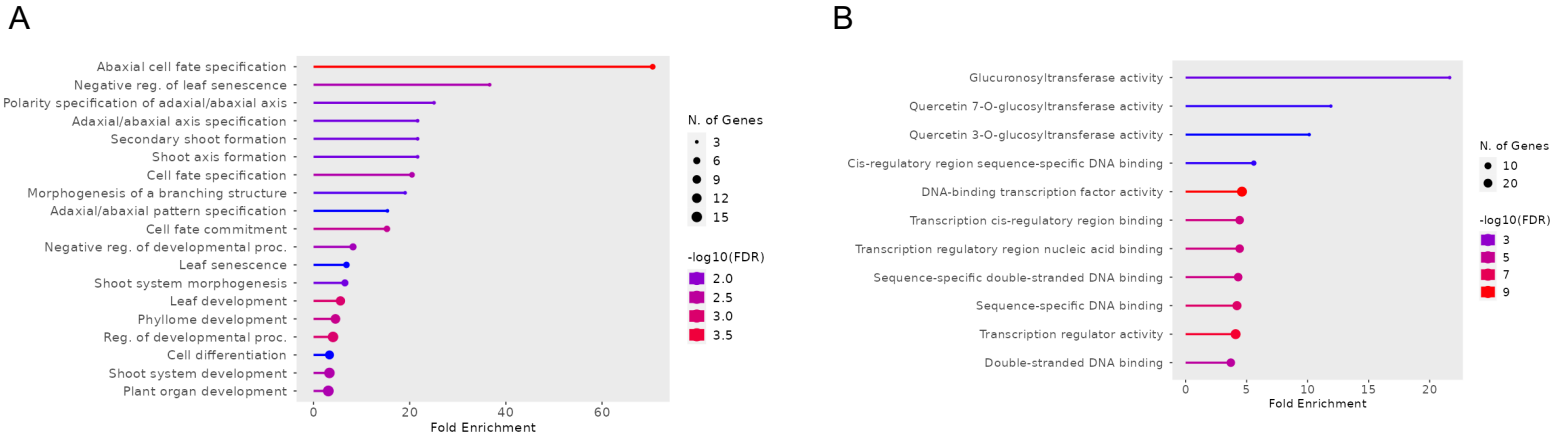

Suppl. Figure S8. Functional categorisation of genes showing a decrease in H3K4me3 levels in *35S::ULT1*.
ShinyGO v0.8 analysis of significantly over-represented Gene Ontology terms among H3K4me3 decreasing genes compared to all H3K4me3 target genes in Ler WT. GO terms are based on **(A)** biological process or **(B)** molecular function.

Suppl. Table S4. Overlaps in H3K27me3 changes caused by ULT1 and Histone Methyl Transferases (HMTs) or Histone DeMethylases (HDMTs). Three tables are displayed, that give, for a derepressive function (_derep) or a repressive function (_rep), (i) the Number of target genes in common, (ii) the Percentage of target genes in common (out of n genes targets of <column>, p % are targets of <line>), (iii) the p-value for the above table and (iv) the Sources for the ChIP-seq dataset used.
JmJ= the three *Arabidopsis thaliana* H3K27 HDMTs: REF6, ELF6, JMJ13.

→ *See excel File*

Suppl. Figure S9

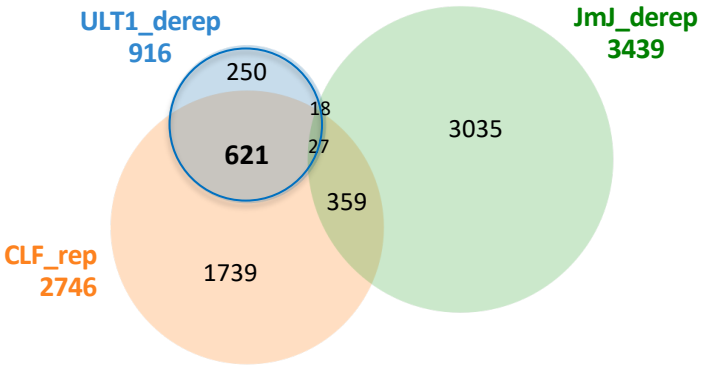

Suppl. Figure S9. Overlap of genes influenced in their H3K27me3 pattern by ULT1, CLF and the three JmJ H3K27me3 HDMT. Venn-diagram showing overlap between populations of ULT1_derep genes with CLF_rep genes (genes with significantly reduced H3K27me3 in *clf*, raw data from Shu *et al.* 2019) and JmJ derep genes (genes with significantly elevated H3K27me3 in *ref6 elf6 jmj13* triple mutant, data from Yan *et al.* 2018).

Suppl. Figure S10

A

ULT1 derepressor (ULT1_K27down list)

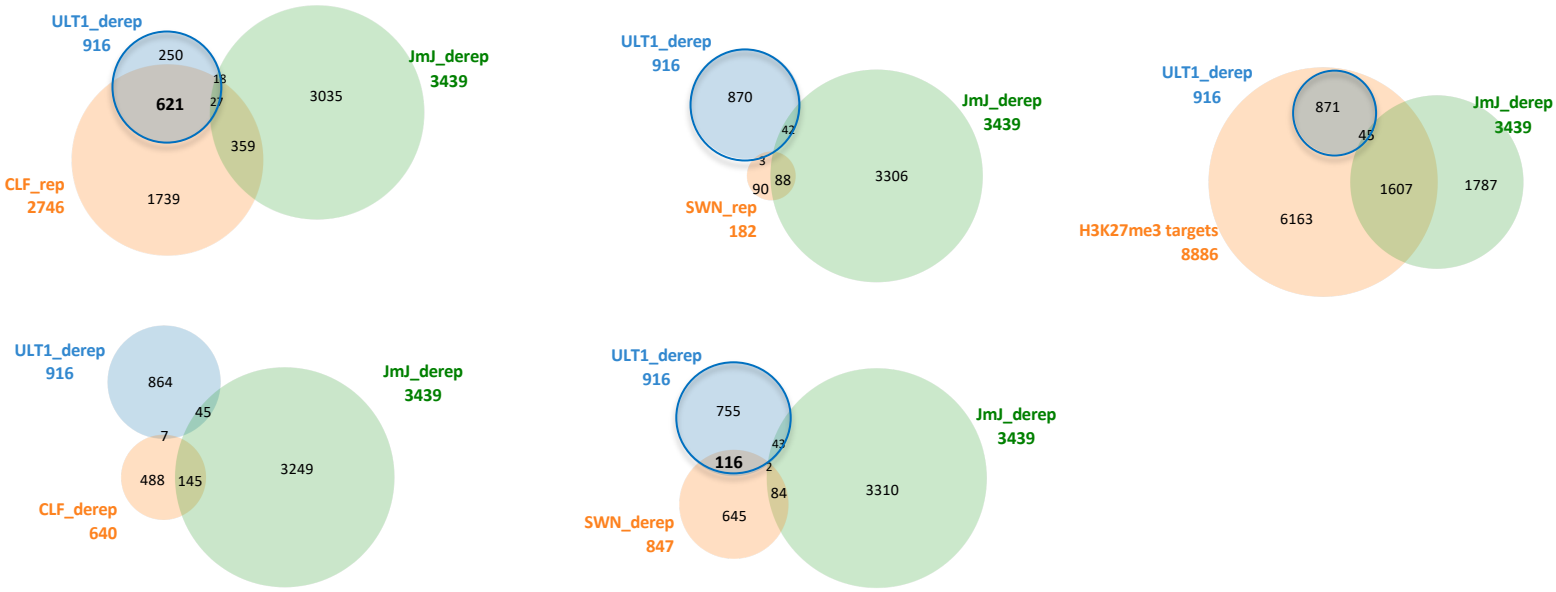

B

ULT1 derepressor (35S::ULT1_K27down list)

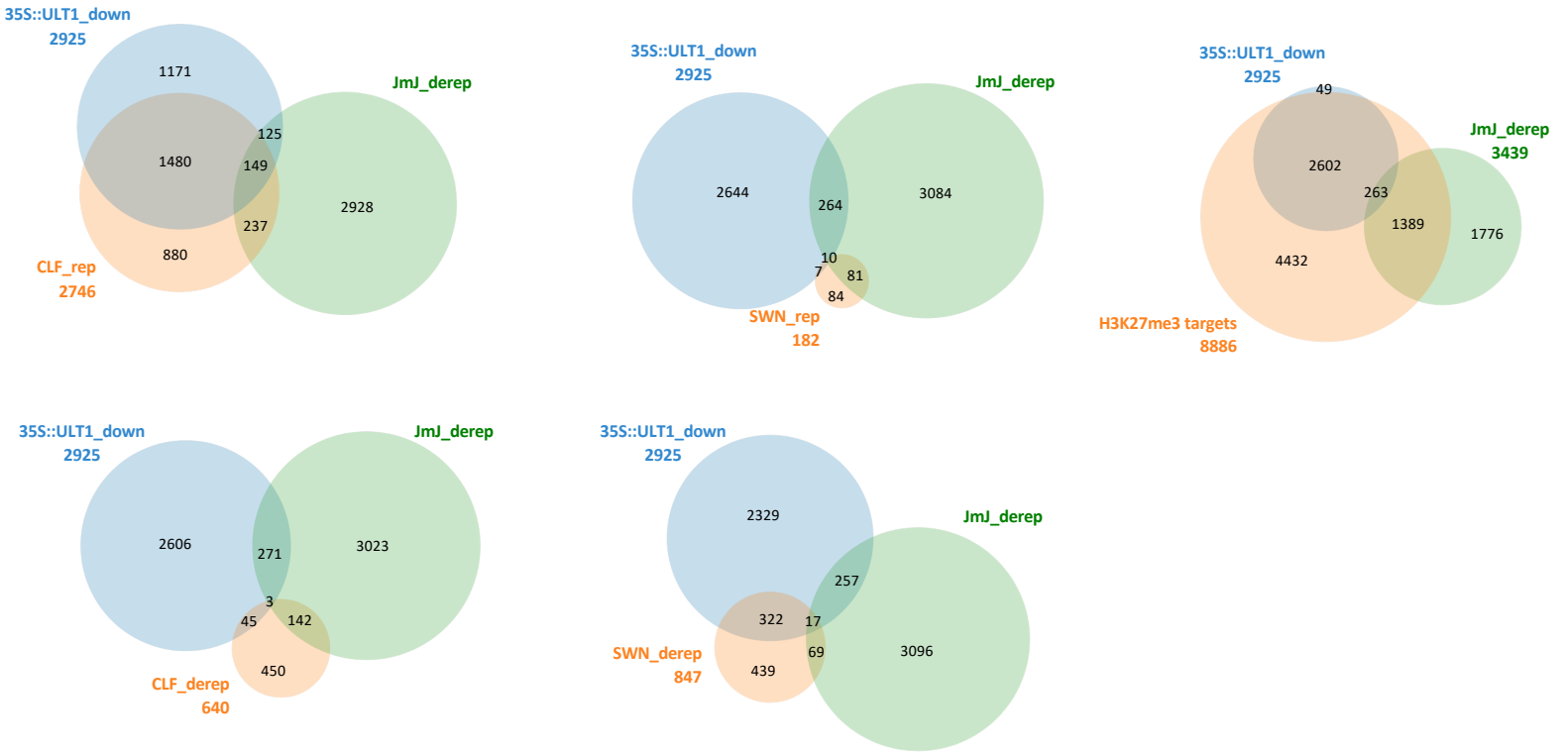

Suppl. Figure S10. Overlap of genes influenced in their H3K27me3 pattern by ULT1, CLF and the JmJ H3K27me3 HDMT (ULT1_derep).
(A) Venn-diagram showing overlap between populations of ULT1_derep genes with genes with significantly deregulated H3K27me3 in *clf*, *swn*, or H3K27me3 marked genes (raw data from Shu *et al*. 2019) and JmJ derep genes (genes with significantly elevated H3K27me3 in *ref6 elf6 jmj13* triple mutant, data from Yan *et al.* 2018).
(B) Venn-diagram showing overlap between populations of 35S::ULT1_down (genes with significantly reduced H3K27me3 in 35S::ULT1) and genes with significantly deregulated H3K27me3 in *clf*, *swn*, or H3K27me3 marked genes and JmJ derep genes (genes with significantly elevated H3K27me3 in *ref6 elf6 jmj13* triple mutant).

Suppl. Figure S11

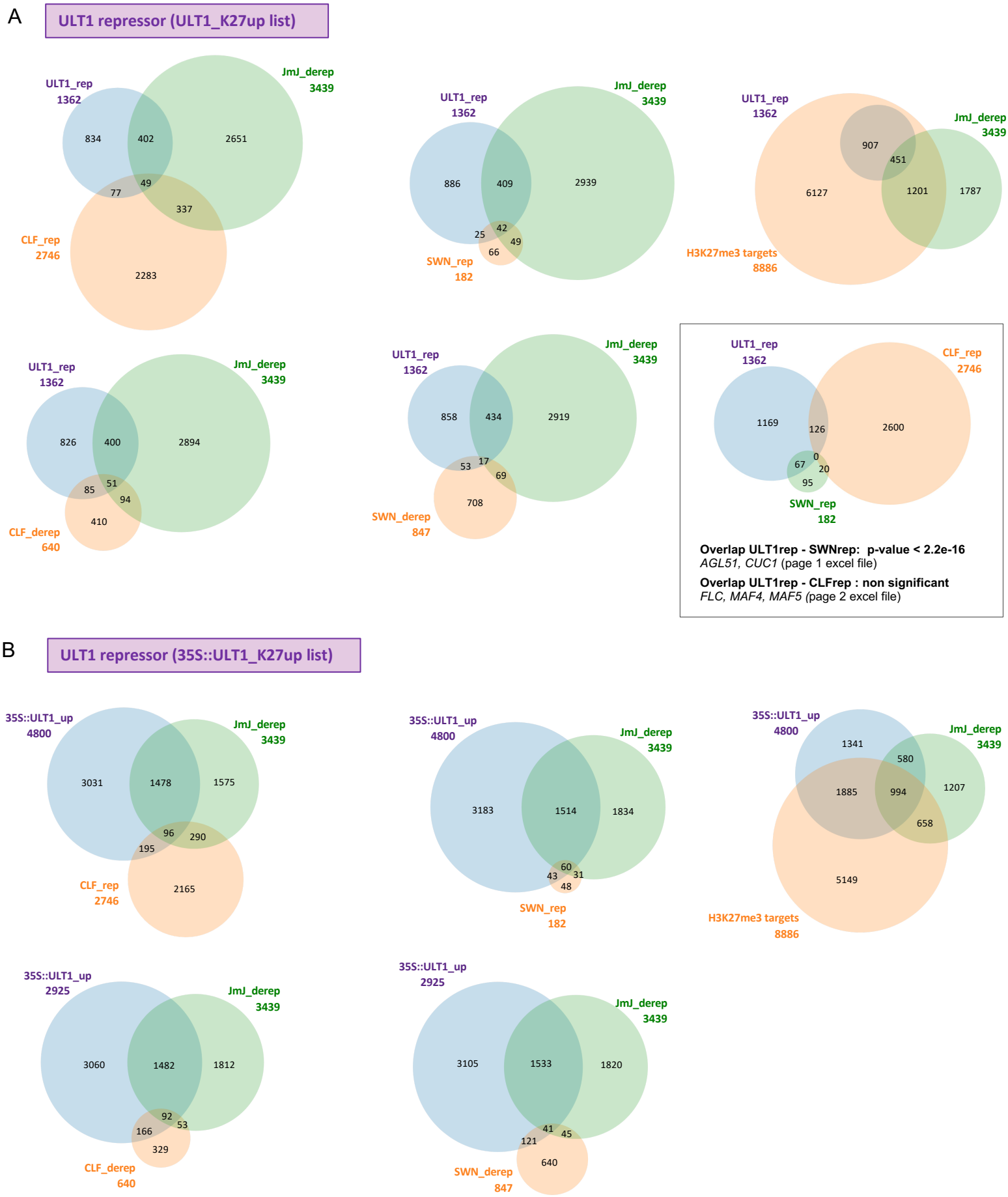

Suppl. Figure S11. Overlap of genes influenced in their H3K27me3 pattern by ULT1, CLF and the three JmJ H3K27me3 HDMT (ULT1_rep). **(A)** Venn-diagram showing overlap between populations of ULT1_rep genes with genes with significantly deregulated H3K27me3 in *clf*, *swn*, or H3K27me3 marked genes (raw data employed from Shu *et al*. 2019) and JmJ derep genes (genes with significantly elevated H3K27me3 in ref6 elf6 jmj13 triple mutant, data from Yan *et al.* 2018). **(B)** Venn-diagram showing overlap between populations of 35S::ULT1_up (genes with significantly increased H3K27me3 in *35S::ULT1*) and genes with significantly deregulated H3K27me3 in *clf*, *swn*, or H3K27me3 marked genes and JmJ derep genes (genes with significantly elevated H3K27me3 in *ref6 elf6 jmj13* triple mutant).

Suppl. Figure S12

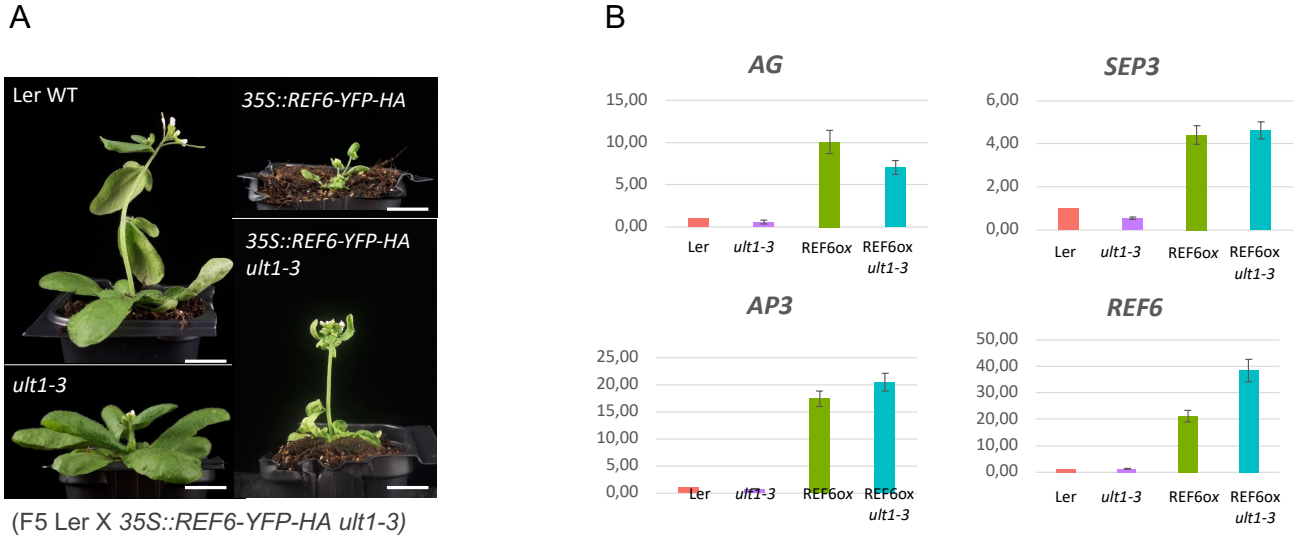

Suppl Figure S12. REF6 is dispensable for ectopic ULT1-induced phenotypes and de-repression of MADS floral genes.
(A) Pictures of 28 day-old Ler plants (WT, *35S::REF6-YFP-HA*, *ult1-3* mutant, *35S::REF6-YFP-HA ult1-3),* indicate that *35S::REF6-YFP-HA* ectopic expression phenotypes do not depend on ULT1 function. **(B)** Relative expression levels of the homeotic floral genes *AG, AP3* and *SEP3,* along with *REF6*, in 8-day-old seedlings, assessed by RT-qPCR. Expression levels of target genes were normalized with the reference gene *MON1*. Error bars correspond to standard errors for 3 technical replicates. Similar results were obtained for 2 biological replicates.

Suppl. Figure S13

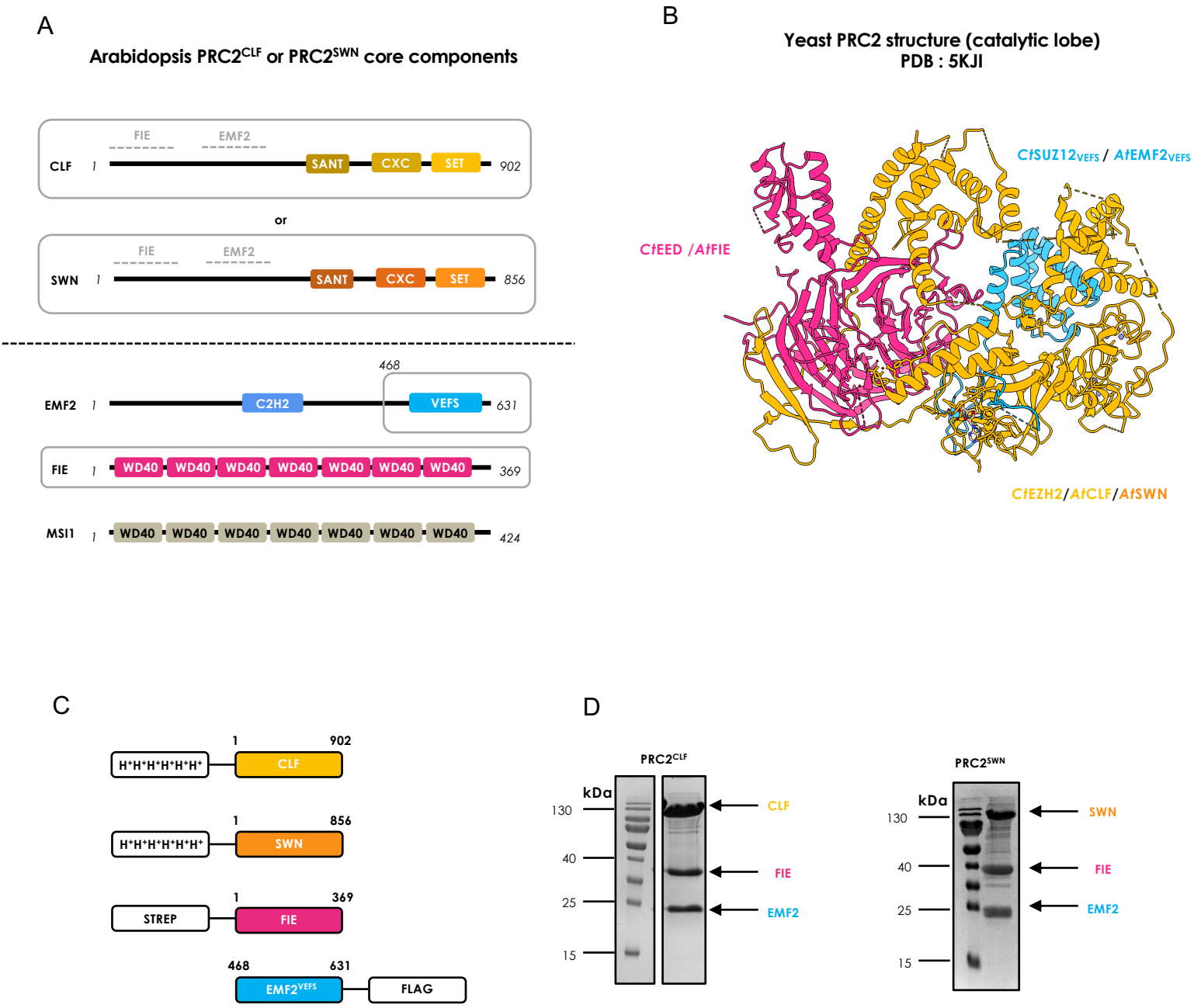

Suppl. Figure S13. Expression strategy for the catalytic lobes of the Arabidopsis PRC2^{CLF} and PRC2^{SWN} complexes.
(A) Schematic representation of the PRC2 complex subunits in *Arabidopsis thaliana*. The catalytic lobe of the PRC2 complex consists of a methyltransferase which is either CLF (yellow) or SWN (orange), the WD40 domain protein FIE (pink) and the VEFS domain of EMF2 (blue). The subunits forming the ternary complex are represented by a grey frame. Areas of interaction of FIE and EMF2 with CLF or SWN are represented by gray bars. The domains of each protein identified using Prosite analysis are represented by coloured rectangles. **(B)** Structure of the catalytic lobe of PRC2 from *Chaetomium thermophilum* determined by X-ray crystallography; PDB: 5KJI (Jiao and Liu, Science 2015) that was used to design the constructs of each subunit. The subunits are represented using the same color code as in (A). **(C)** Schematic representation of the constructs made for each subunit of the PRC2 complex. The coding sequences for CLF$_{1\text{-}902}$ (or SWN$_{1\text{-}856}$), FIE$_{1\text{-}369}$ and EMF2$_{468\text{-}631}$ were cloned into expression vectors for production of recombinant proteins in fusion with His$_6$, Strep or Flag tags, respectively. The complex purification tags associated with each subunit and their positions (N-terminal or C-terminal) are indicated. **(D)** SDS-PAGE of the PRC2^{CLF} and PRC2^{SWN} complexes after purification by size exclusion chromatography.

Suppl. Figure S14

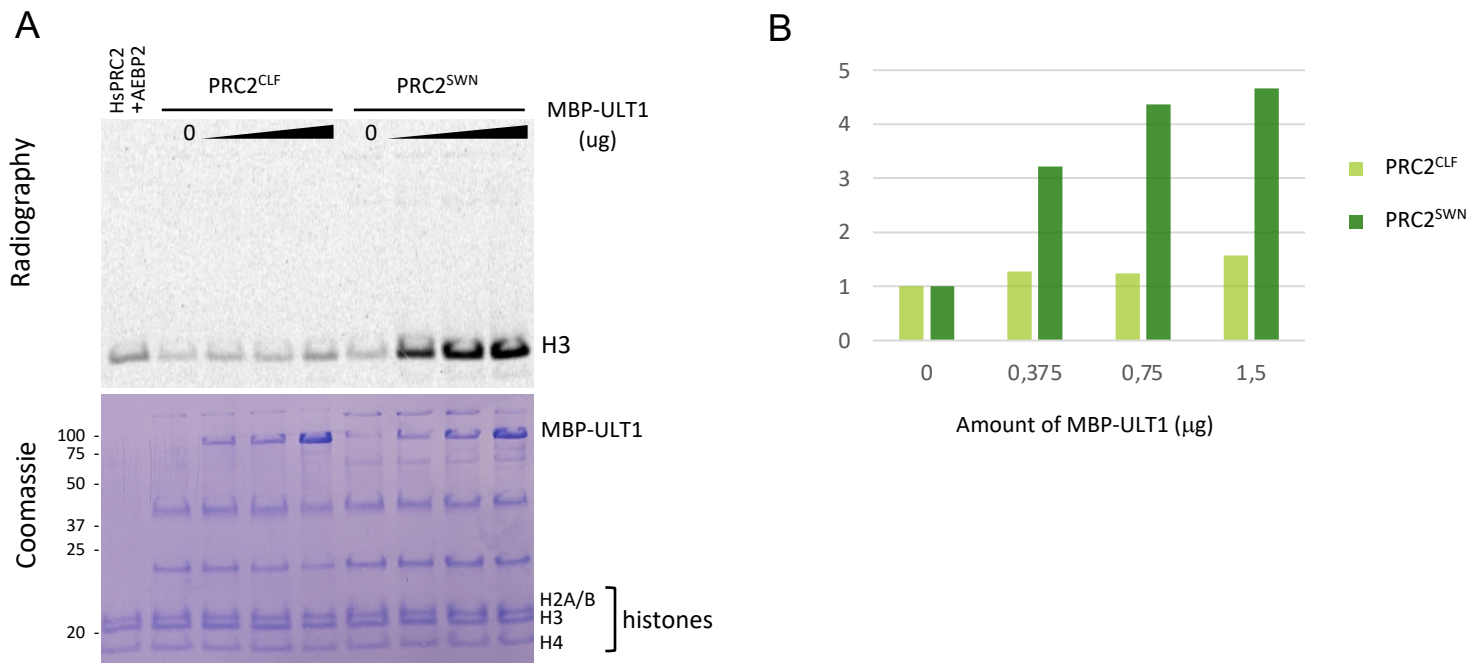

Suppl. Figure S14. *In vitro* HMT activity tests show ULT1-mediated increase of the PRC2^{SWN} activity but not of the PRC2^{CLF} activity.

(A) Top panel shows autoradiography of a SDS-PAGE gel after incubation of PRC2^{CLF} or PRC2^{SWN} (1.5ug of complex) without or with ULT1 in increasing amounts (0, 0.375, 0.75, 1.5ug). The HsPRC2 complex (0.5ug) was loaded in the first lane after incubation with the cofactor AEBP2, for positive control. Bottom panel shows Coomassie staining of the same SDS-PAGE. **(B)** Graph showing relative quantifications of HMT activities for PRC2^{CLF} and PRC2^{SWN} incubated with MBP-ULT1.

Suppl. Figure S15

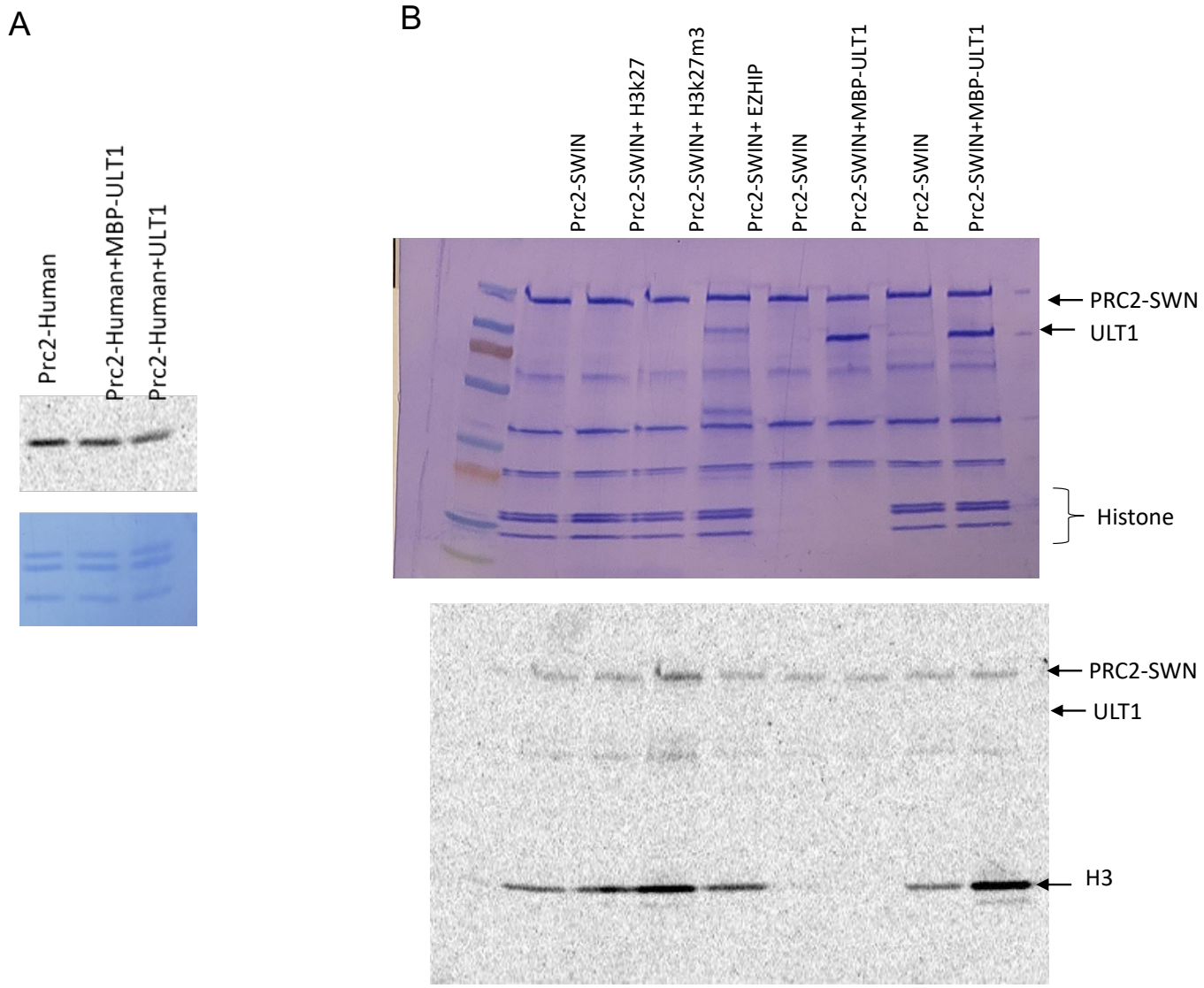

Suppl. Figure S15. *In vitro*, ULT1 does not impact the activity of the HsPRC2 EZH2 complex and is not methylated by PRC2^{SWN}.
(A) When added to the HsPRC2 EZH2 complex, ULT1 does not impact its HMT activity.
(B) ULT1 is not methylated by PRC2^{SWN}, the H3K27me3 peptide increases PRC2^{SWN} enzymatic activity, and the Ezhip peptide known for inhibiting HsPRC2**,** does not inhibit PRC2^{SWN} activity (1.5ug of complex). Top panel shows Coomassie staining of the SDS-PAGE correspondig to the autoradiography below.
This dataset indicates that ULT1 functions differently from the JARID cofactor of human PRC2.

Suppl. Figure S16

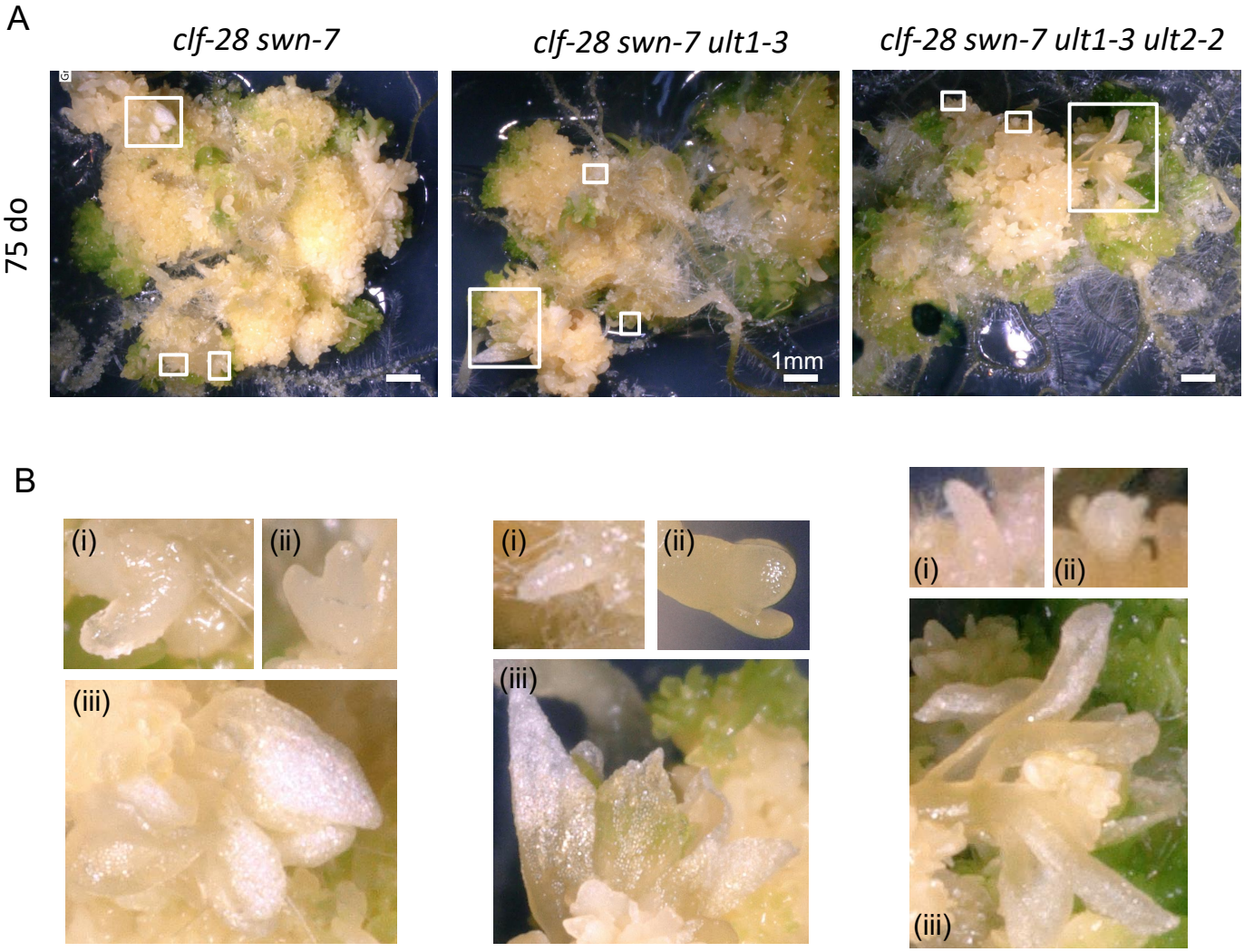

Suppl. Figure S16. *ult* loss-of-function does not complement sporophytic *prc2* mutant phenotypes.
(A) Pictures of double *clf-28 swn-7, triple clf-28 swn-7 ult1-3* and quadruple *clf-28 swn-7 ult1-3 ult2-2* mutants grown on MS agar plates for 2.5 months. All genotypes grow as callus-like tissue with random organs arising in a disorganised phyllotaxy. **(B)** Magnified views of insets drawn in panels shown in (A), showing ectopic (i) roots and hair roots, (ii) somatic embryos or shoot apex-like structure, and (iii) developed shoots with some homeotic conversions to floral organ types. Scale bar: 1mm.

Suppl. Figure S17

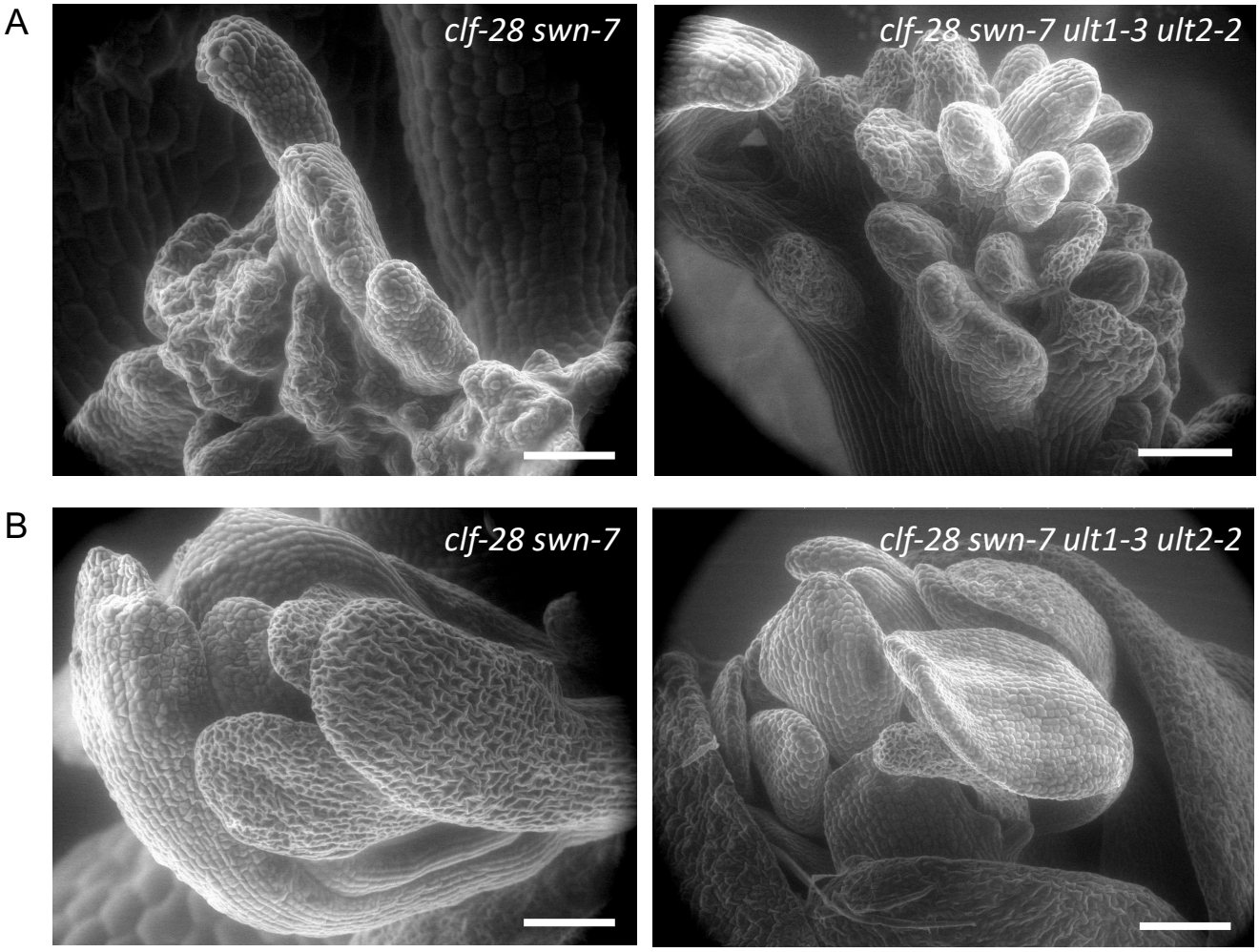

Suppl. Figure S17. SEM images of *clf-28 swn-7* and *clf-28 swn-7 ult1-3 ult2-2* loss-of-function lines show stigmatic papillae-type outgrowths and growth of flower-like structures. Pictures of double *clf-28 swn-7* and quadruple *clf-28 swn-7 ult1-3 ult2-2* mutants grown on MS agar plates for 3 weeks. **(A)** Ectopic stigmatic papillae-like outgrowths. **(B)** Organs arranged in flower-like structures. Scale bar: 100um.

Suppl. Figure S18

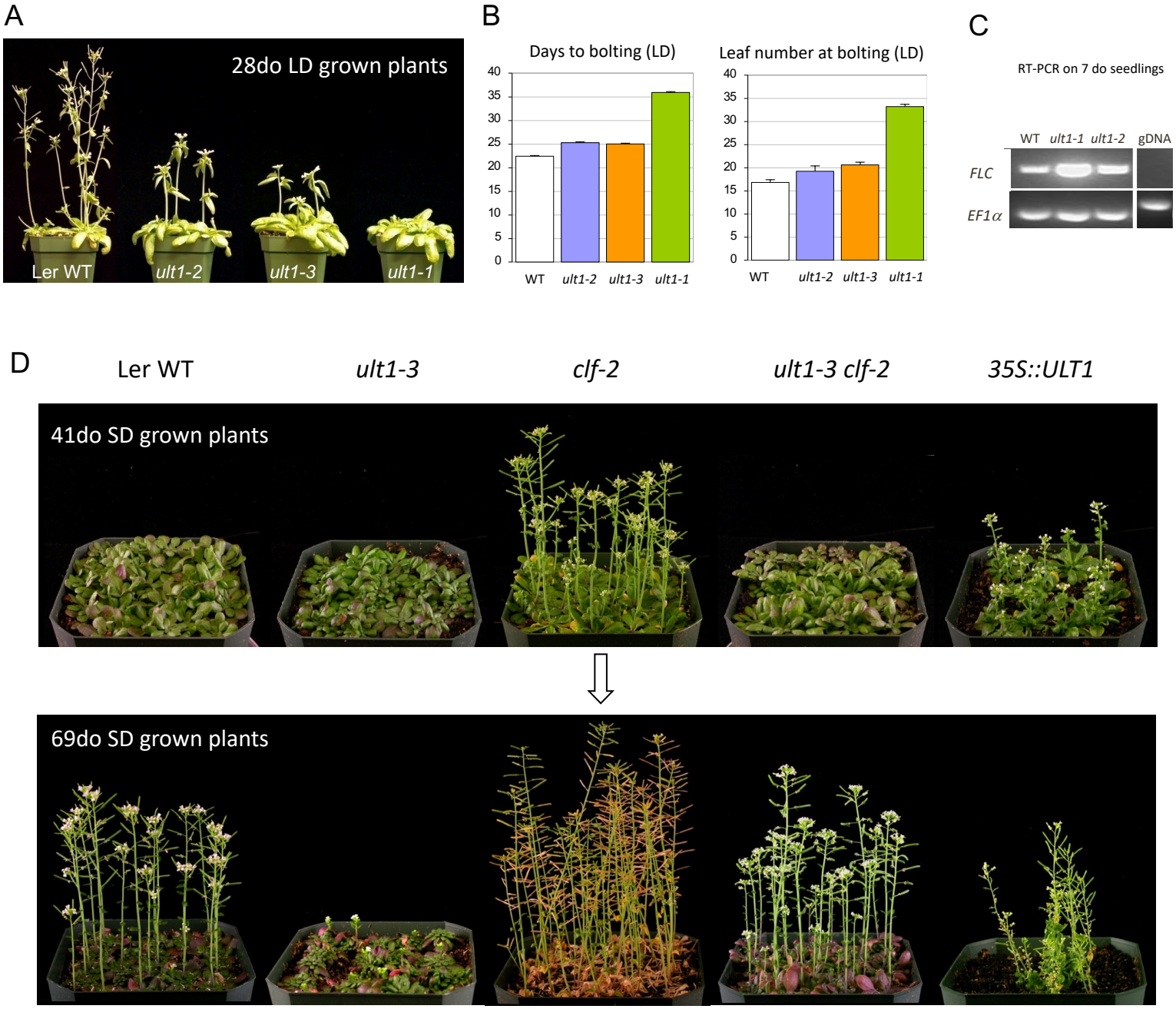

Suppl. Figure S18. Flowering time of ULT1 lof and gof plants in the Ler ecotype, in LD and SD.

(A-C) Plants grown in LD condition. (A) Representative 28 day-old Ler WT, *ult1-2, ult1-3* and *ult1-1* mutant plants grown at 20 ° C in long days. **(B)** Number of days to bolting and number of rosette leaves were scored as proxy for the flowering time. The previously reported semi-dominant *ult1-1* mutant allele exibits a more dramatic late flowering phenotype than the null *ult1-2* and *ult1-3* alleles. **(C)** RT-PCR performed on 7 day-old plants reveals a high upregulation of *FLC* expression.

(D) Plants grown in SD condition. Representative Ler WT, *ult1-3, clf-2, ult1-3 clf-2* and *35S::ULT1* plants grown at 20 ° C in short days were pictured at 41 and 69 days old.

Suppl. Figure S19

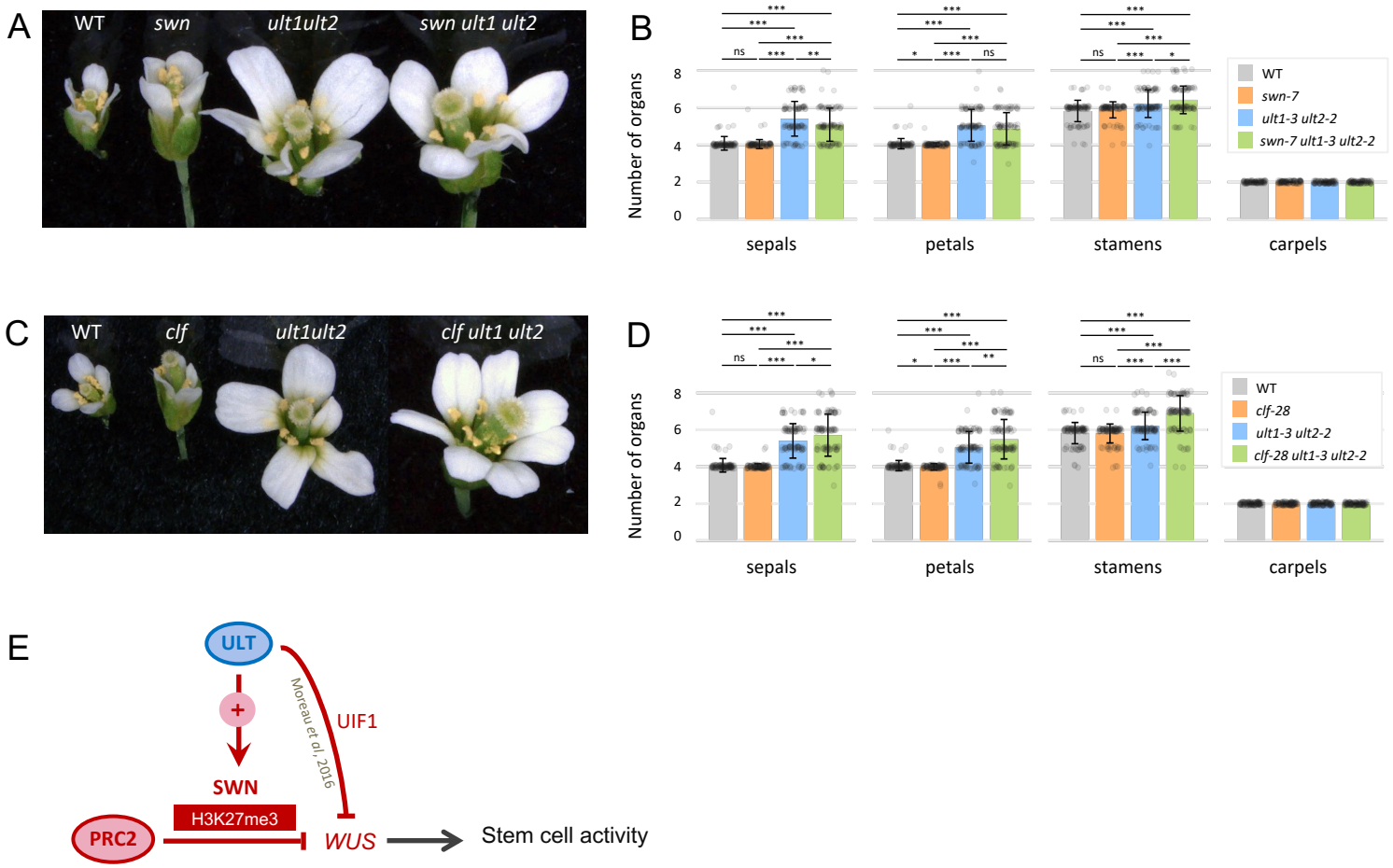

Suppl. Figure S19. Genetic interactions between ULT and sporophytic PRC2 functions for flower meristem maintenance.
(A) Representative flowers of Col-0 WT, *swn-7, ult1-3 ult2-2* and *swn-7 ult1-3 ult2-2* plants. **(B)** Organ numbers in each floral whorl, for all above mentioned genotypes. Flowers of *ult1 ult2 swn* triple mutant produce the same number of organs as flowers of *ult1 ult2* double mutants , for each whorl.
(C) Representative flowers of Col-0, *clf-28, ult1-3 ult2-2* and *clf-28 ult1-3 ult2-2* mutant plants. **(D)** Organ numbers in each floral whorl, for all above mentioned genotypes. Flowers of *ult1 ult2 clf* triple mutant produce more floral organs than *ult1 ult2* double mutants, indicating a synergy between ULT and CLF pathways.
In B,C: n (number of counted flowers) = 100 for all genotypes except for *swn-7 ult1-3 ult2-2* (n=99). p-values are as follows: * $p < 0.05$, ** $p < 0.01$, *** $p < 0.001$, ns = not significant.
(E) Working model for stem cell activity at the floral meristem, and for *WUS* regulation by ULT1 and PRC2. ULT1 functions together with SWN to promote *WUS* repression. Moreover, another pathway could be considered for ULT, independent of PRC2, involving a direct interaction with the UIF1 transcription factor which has a repressive function on *WUS* expression (Moreau *et al.*, 2016).

Suppl. Table S5. List and sequences of primers used in this study.

→ *See excel File*